DNA damage signaling in *Drosophila* macrophages modulates systemic cytokine levels in response to oxidative stress

Authors: Fabian Hersperger[1,2], Tim Meyring[1], Pia Weber[1], Chintan Chhatbar[1], Gianni Monaco[1,3], Marc S. Dionne[4,5], Katrin Paeschke[6,7], Marco Prinz[1,8,9], Olaf Groß[1,8,9], Anne-Kathrin Classen[10,11] & Katrin Kierdorf[1,8,11#]

[1] Institute of Neuropathology, Faculty of Medicine, Medical Center, University of Freiburg, Freiburg, Germany

[2] Faculty of Biology, University of Freiburg, Freiburg, Germany

[3] Institute for Transfusion Medicine and Gene Therapy, Medical Center-University of Freiburg, Freiburg, Germany

[4] MRC Centre for Molecular Bacteriology and Infection, Imperial College London, London, United Kingdom

[5] Department of Life Sciences, Imperial College London, London, United Kingdom

[6] Department of Oncology, Haematology and Rheumatology, University Hospital Bonn, Venusberg-Campus 1, Bonn, Germany

[7] Institute of Clinical Chemistry and Clinical Pharmacology, University Hospital Bonn, Bonn, Germany

[8] Center for Basics in NeuroModulation (NeuroModulBasics), Faculty of Medicine, University of Freiburg, Freiburg, Germany

[9] Signalling Research Centres BIOSS and CIBSS, University of Freiburg, Freiburg, Germany

[10] Hilde-Mangold-Haus, Faculty of Biology, University of Freiburg, Freiburg, Germany

[11] CIBSS-Centre for Integrative Biological Signalling Studies, University of Freiburg, Freiburg, Germany

#corresponding author: katrin.kierdorf@uniklinik-freiburg.de

Summary

Environmental factors, infection, or injury can cause oxidative stress in diverse tissues and loss of tissue homeostasis. Effective stress response cascades, conserved from invertebrates to mammals, ensure reestablishment of homeostasis and tissue repair. Hemocytes, the *Drosophila* blood-like cells, rapidly respond to oxidative stress by immune activation. However, the precise signals how they sense oxidative stress and integrate these signals to modulate and balance the response to oxidative stress in the adult fly are ill-defined. Furthermore, hemocyte diversification was not explored yet on oxidative stress. Here, we employed high throughput single nuclei RNA-sequencing to explore hemocytes and other cell types, such as fat body, during oxidative stress in the adult fly. We identified distinct cellular responder states in plasmatocytes, the *Drosophila* macrophages, associated with immune response and metabolic activation upon oxidative stress. We further define oxidative stress-induced DNA

damage signaling as a key sensor and a rate-limiting step in immune-activated plasmatocytes controlling JNK-mediated release of the pro-inflammatory cytokine *unpaired-3*. We subsequently tested the role of this specific immune activated cell stage during oxidative stress and found that inhibition of DNA damage signaling in plasmatocytes, as well as JNK or upd3 overactivation, result in a higher susceptibility to oxidative stress. Our findings uncover that a balanced composition and response of hemocyte subclusters is essential for the survival of adult *Drosophila* on oxidative stress by regulating systemic cytokine levels and cross-talk to other organs, such as the fat body, to control energy mobilization.

Keywords: hemocytes; plasmatocytes; *Drosophila* macrophages; oxidative stress; macrophage-derived cytokines; DNA damage; unpaired-3

Introduction

Metazoan organisms must constantly adapt to the surrounding environment. Environmental factors, including radiation, pathogens or toxins, permanently lead to the generation of reactive oxygen species (ROS)[1]. In vertebrates and invertebrates, low levels of ROS support cellular pathways like immune cell differentiation and even immune function including antimicrobial defense[2,3]. At high concentrations, ROS lead to oxidative stress, a deleterious process that negatively impacts protein synthesis and stability, lipid metabolism as well as overall genome stability. ROS mediated cellular damage can further result in degenerative diseases or cancer[4]. Therefore, metazoan organisms employ efficient repair and defense mechanisms to circumvent high levels of oxidative stress and subsequent organ damage. Hence, keeping the balance between the production and the antioxidant-dependent clearance of ROS is essential for the survival and well-being of the affected organism[5]. Oxidative stress induced tissue damage is most often followed by a strong local immune response. These molecular processes are conserved across vertebrates and invertebrates such as the fruit fly *Drosophila melanogaster*[6].

Hemocytes, the *Drosophila* blood cells, are essential cellular components of the immune and stress response machinery. They consist of three different subtypes: crystal cells, lamellocytes and plasmatocytes[7]. Plasmatocytes are considered to be macrophage equivalents in *Drosophila* and comprise up to 95 % of all hemocytes in the adult fly[8]. They share many functions as well as the multilayered ontogeny with vertebrate tissue macrophages[9,10]. Adult plasmatocytes are actively involved in many immune functions such as pathogen recognition, defense and phagocytosis but also chronic immune activation upon metabolic stress by dietary lipids[11,12]. Recent studies highlighted the essential role of adult plasmatocytes as key players in regulation of tissue homeostasis, including the gut by regulating the intestinal stem cell niche or in muscles by controlling glucose homeostasis[13,14].

Similar to higher eukaryotes, levels of ROS are used as a central antimicrobial defense mechanism of hemocytes against invading pathogens[15]. Moreover, larval hemocytes respond differentially to ROS, with two cell subsets mounting a biphasic immune reaction to invading bacteria by controlling hemocyte spreading and adhesion as well as crystal cell rupture[15]. Larval hemocytes have been also attributed to respond to increased oxidative stress of other tissues, as seen in response to oxidative stress in the eye-antenna imaginal disc[16]. Similarly, by regulating the intestinal stem cell (ISC) proliferation in the damaged midgut during infection-induced or chemical-induced oxidative stress[14], adult hemocytes were described to release the bone morphogenetic protein (BMP) homologue *decapentaplegic* (*dpp*) to facilitate tissue repair[14]. Other studies pointed to an essential role of hemocyte-derived *unpaired-3* (*upd3*), which is the *Drosophila* orthologue of Interleukin-6, in the regulation of ISC proliferation during septic injury[17], as well as wound healing during sterile injury[18]. In line with these findings, hemocytes have been implicated in organ-to-organ immune signaling for example upon infection-induced injury in the gut and antimicrobial peptide (AMP) production in the fat body[19]. Hemocyte activation is thus a hallmark of oxidative stress in defined tissues, though their role in modulating and controlling oxidative stress response to facilitate tissue repair and survival of the organism remains undefined.

Here, we demonstrate an essential role of hemocytes to control susceptibility to oxidative stress, where hemocytes orchestrate systemic oxidative stress response by defined cellular states identified by unbiased transcriptomic profiling. Plasmatocytes segregate in oxidative stress responder subclusters, characterized by immune activation and cellular stress response, and potential bystander subsets associated with metabolic gene regulations. Mechanistically, we unravel that the direct immune response to oxidative stress by plasmatocytes is driven by c-Jun N-terminal kinase (JNK) and Jak/STAT pathway activation with subsequent induction of the pro-inflammatory cytokine *upd3*. This inflammatory cascade is to a certain amount regulated by DNA damage signaling in plasmatocytes and essentially defines the susceptibility of the fly to oxidative stress. Deficiencies in the DNA damage signaling machinery in plasmatocytes lead to elevated JNK activation, cytokine release and subsequently a higher susceptibility of the adult fly to oxidative stress. Hence, our data point to a key role of plasmatocytes in balancing systemic cytokine levels and stress response upon oxidative stress. Collectively we provide new insights on the role of macrophages in orchestrating systemic stress responses in other tissues and to balance tissue wasting and energy mobilization.

Results

Hemocytes control susceptibility to oxidative stress

104 In vertebrates and invertebrates, prolonged oxidative stress can cause severe tissue damage, hence
105 controlled activation of stress signaling cascades are essential for the survival of the organism and the
106 resolution of oxidative stress with subsequent tissue repair. Yet the precise role of macrophages in the
107 initiation and control of oxidative stress signaling needs to be determined.

108 To analyze the role of macrophages in signaling cascades to oxidative stress, we took advantage of the
109 well-established Paraquat (PQ)-feeding model in adult *Drosophila melanogaster* to induce systemic
110 oxidative stress[20]. Feeding of 7-days old *w;Hml-Gal4,UAS-2xeGFP/+* (*Hml/+*) flies with PQ-
111 supplemented sucrose solution led to an increased lethality of adult *Drosophila* after 18 hours in a
112 dose dependent manner (0mM: 1.25 ± 1.25 %, 2mM: 2.5 ± 1.6 4%, 15mM: 27.78 ± 5.47 %, and 30mM:
113 38.75 ± 6.67 %) (Figure S1A). In agreement with previous studies[20], 15mM PQ was chosen for further
114 experiments (Figure 1A). First, we determined which systemic changes are associated with
115 susceptibility to oxidative stress. Infection induced damage in enterocytes can result in gut leakage and
116 subsequent death[17]. We tested if the death of flies after 18 hours on 15mM PQ food was associated
117 with PQ-induced damage of gut enterocytes and resulting gut leakage, but we found no indication of
118 gut leakage on 15mM PQ food (Figure S1B). Only very few flies on control food and PQ indicated gut
119 leakage of the food color to thorax and abdomen which was unrelated to the treatment and not altered
120 between the groups (control: 3.75%, 2mM PQ: 2.53 %, 15mM PQ: 1.11 % and 30mM PQ: 3.75 %)
121 (Figure S1B). We investigated if aberrant systemic induction of immune signaling cascades are seen
122 upon PQ-mediated oxidative stress. For this, gene expression levels of different known immune
123 activated genes were analyzed by qPCR such as *unpaired* (*upd*) cytokines (*upd1*, *upd2*, *upd3*), *Jak/STAT*
124 down-stream targets (*Turandot-A* (*TotA*), *suppressor of cytokine signaling at 36E* (*Socs36E*)), stress
125 induced JNK activation (*puckered* (*puc*)) (Figure 1B), as well as expression of *nuclear factor 'kappa-light-*
126 *chain-enhancer' of activated B-cells* (*Nfkb)*-induced antimicrobial peptides (AMP) and further cytokines
127 such as *eiger*, *dpp* and *dawdle* (*daw*) (Figure S1C-D). These analyses did not reveal significant
128 differences for these gene groups on a systemic level. In contrast, genes associated with carbohydrate
129 metabolism such as *insulin receptor* (*InR*), *phosphoenolpyruvate carboxykinase* (*Pepck*), and *Thor* were
130 significantly upregulated upon PQ-feeding (Figure 1C). These findings point to an activation of *forkhead*
131 *box, sub-group O* (*foxo)*-target genes and a potentially reduced insulin signaling, despite the lack of
132 significant alterations in the expression of the Insulin-like peptides (*Ilps*) *Ilp2*, *Ilp3* and *Ilp5* (Figure 1C).

133 To test the consequences for energy mobilization and nutrient storage, we measured free glucose
134 content, as well as glycogen and triglyceride levels in whole flies after 18 hrs on control or 15mM PQ.
135 Although no changes in free glucose levels (control: 1.49±0.02µg and PQ: 1.50±0.07µg, ns p=0.954)
136 (Figure 1D) were found, we observed a clear decrease in stored glycogen (control: 1.02±0.07µg and
137 PQ: 0.33±0.08µg, ***p=0.003*) (Figure 1E) and stored triglycerides (Figure 1F) in PQ-treated flies
138 compared to control. Next, we examined histological sections of flies to define which tissues might be

139 affected. Hematoxylin and eosin (H&E) and Oil Red O (ORO) stainings showed a shrinkage in fat body
140 cell size and stored lipid-filled vesicles in the abdominal fat body compared to flies kept under control
141 conditions (Figure S1E-F). Fat body development, energy mobilization and storage have been recently
142 connected to the presence, cell number and subsequent cross-talk of hemocytes with fat body[21],
143 therefore we quantified GFP^+ hemocytes in *Hml/+* flies after 18 hrs on PQ or control food (Figure 1G-
144 H). Our analysis did not reveal alterations in hemocyte numbers and especially no oxidative stress
145 induced loss of hemocytes (control: 243.4±24.33 hemocytes per fly and PQ: 219.6±24.22 hemocytes
146 per fly, ns *p=0.508*) (Figure 1G-H). To evaluate if hemocytes are essential contributors to the stress-
147 mediated metabolic changes and susceptibility to oxidative stress, we used "hemocyte-deficient" *crq-*
148 *Gal80^{ts}>reaper* (*w;tub-Gal80ts/UAS-CD8-mCherry;crq-Gal4/UAS-reaper*) flies and tested their survival
149 rate compared to control flies on PQ food (Figure 1I). Hemocyte-deficient flies displayed a significantly
150 higher mortality rate on 15mM PQ (43.33±6.30%) compared to control flies (13.08±2.63%) (Figure 1I).
151 Next, we analyzed triglycerides, as well as free glucose and glycogen levels in whole flies after 18 hrs
152 on control or 15mM PQ. Interestingly, we found that hemocyte-deficient flies compared to the control
153 genotype mobilized less triglycerides from the fat body during oxidative stress (Figure 1J). When we
154 looked into free glucose levels, we found that these flies show a decrease in free glucose upon PQ
155 feeding, whereas the control genotype showed similar free glucose levels as on normal food (Figure
156 1K). In contrast we did not detect any difference in glycogen levels between the two genotypes on
157 control food and on PQ food (Figure 1L). Our findings show detrimental changes in energy mobilization
158 upon oxidative stress in the absence of profound systemic overactivation of immune signaling
159 cascades, however the presence or absence of hemocytes seem to be a key determinant of the
160 susceptibility to oxidative stress and results in altered energy mobilization in adult *Drosophila*. This
161 strongly points to an essential role for hemocytes in controlling stress response and organismal survival
162 upon oxidative stress.

163 **Paraquat exposure generates diverse transcriptional states of adult hemocytes with a specific cell**
164 **state associated with oxidative stress response**

165 To gain further insights into the alterations induced in the adult fly upon oxidative stress and especially
166 to the hemocyte compartment, we decided to take advantage of unbiased single nucleus RNA-
167 sequencing (snRNA-seq). We isolated nuclei from control food and PQ-treated *Hml-DsRed.nuc* flies
168 with a modified Frankenstein protocol[22] and performed fluorescence activated nuclear sorting of
169 $DAPI^+Draq7^+$ nuclei (Figure S2A). From two independent sorts we obtained a total of 29000 nuclei
170 which were utilized for subsequent droplet-based barcoding of single nuclei, and generation of single
171 nucleus cDNA libraries. We could successfully obtain gene expression data from 11839 nuclei (Figure
172 S2B-D). Quality control analysis followed by unsupervised hierarchical clustering of all analyzed nuclei

173 using Seurat package[23] revealed 20 distinct nuclei clusters (C) with differential gene expression (Figure
174 2A). Cell identity was annotated according to the cell type-specific signatures determined by the Fly
175 Cell Atlas consortium (Figure 2A)[24]. All annotated cell types were detected in PQ-treated and control
176 flies (Figure 2B).

177 Using cell type-specific signatures, three of the clusters were annotated as hemocytes (clusters: 2, 11
178 and 14) (Figure 2A-B). Re-scaling and clustering of all 1354 identified hemocyte nuclei revealed 8
179 distinct clusters (Figure 2C). We verified hemocyte-specific signature genes across these clusters
180 including genes such as the transcription factor *Serpent* (*Srp*) and one or more of the following
181 hemocyte signature genes: *Hemolectin* (*Hml*), *croquemort* (*crq*), *Nimrod C1* (*NimC1*), *eater,* and
182 *Peroxidasin* (*Pxn*) (Figure S3A-L)[25,26]. Cluster 8 expressed various crystal cell-specific markers including
183 *lozenge* (*lz*), *pebbled* (*peb*), *prophenoloxidase 1* (*PPO1*), and *prophenoloxidase* 2 (*PPO2*), whereas all
184 other clusters seemed to be plasmatocytes (Figure S3A-L). In line with previous reports, the embryonic
185 and larval hemocyte markers *Hemese* (*He*) (data not shown) and *singed (sn)* were not expressed across
186 any of the identified clusters (Figure S3H). Interestingly, when we defined which hemocyte clusters
187 were enriched in control flies or PQ-treated flies, the two plasmatocyte clusters C1 and C7 were
188 primarily derived from control flies, whereas C2, C3, C4 and C6 are predominantly found in PQ-treated
189 flies (Figure 2D and Figure S3M). The plasmatocyte cluster C5 as well as the crystal cell cluster C8
190 presented in both conditions to similar proportions (Figure 2D and Figure S3M).

191 Next, we analyzed the TOP20 differentially expressed (DE) genes across all hemocyte clusters. We
192 found clear differences between the 7 distinct plasmatocyte clusters and the crystal cell cluster (Figure
193 2E and Table S1). The crystal cell cluster C8 showed a high expression of crystal cell specific genes
194 including *lz*, *peb*, *PPO1* and *PPO2* (Figure 2E). Plasmatocyte cluster C1, which was mostly present in
195 control conditions, had a remarkable expression of hemocyte specific marker genes such as *Hml* and
196 *Pxn,* as well as migration-associated genes including the semaphorins *Sema2a and Sema5c* (Figure 2E).
197 Yet this cluster also showed higher expression of genes contributing to metabolic regulations such as
198 the L-gulonate 3-dehydrogenase *Had2* and the gluconolactonase *regucalcin* (Figure 2E). The cluster C7
199 and C1, mostly found in control flies, substantially shared gene expression profiles. In contrast, cluster
200 C2 and C3 were nearly exclusively found in PQ-treated flies and showed expression of genes involved
201 in metabolic adaptations. Due to this finding we verified that these cell clusters are *bona fide*
202 hemocytes and not fat body cells. We analyzed the expression of characteristic fat body signature
203 genes, such as *Trehalose-6-phosphate synthase 1* (*Tps1*), *CG16758*, *CG2233*, *CG4716*, *Ultrabithorax*
204 (*Ubx*), *Calcium/calmodulin-dependent protein kinase I* (*CaMKI*), *Desaturase 1* (*Desat1*), *Phosphoribosyl*
205 *pyrophosphate synthetase* (*Prps*), *CG34166* and *Apolipoprotein lipid transfer particle* (*Apoltp*) across all
206 identified hemocyte clusters (Figure S4A). Metabolic adaptation within these clusters included high

207 expression of the *glucose transporter 4 enhancer factor* (*Glut4EF*) or the *phosphatidate phosphatase*
208 *Lipin* (*Lpin*) in C2 or the induced expression of the lipase *brummer* (*bmm*), the autophagy-associated
209 gene *Atg17* or the *lipophorin receptor LpR1*, involved in uptake of neutral lipids from the hemolymph,
210 in C3 (Figure 2E). Overall gene expression profiles in clusters C2 and C3 showed an induction of insulin
211 signaling, increased autophagy and lipolysis pointing to adaptation of energy mobilization in these
212 clusters upon PQ treatment (Figure 2E). Cluster C4 was characterized by a remarkable upregulation of
213 genes involved in translation including many ribosomal proteins such as *RpL8*, *RpL31* or *RpS13* (Figure
214 2E). Furthermore, C4 included genes associated with unsaturated fatty acid metabolism such as
215 *Desaturase 1 (Desat1)*. Similarly, cluster C5 also showed induction of genes involved in fatty acid
216 metabolism such as *ELOVL fatty acid elongase 7* (*ELOVL*) (Figure 2E). Of note, we also found *Tie-like*
217 *receptor tyrosine kinase* (*Tie*) specifically expressed in this cluster, which is described to bind PDGF-
218 and VEGF-related factor (Pvf) ligands and contribute to cell survival and migration, as well as actin-
219 associated binding proteins including *polychaetoid* (*pyd*) and *formin 3* (*form3*). All these gene
220 expression changes are pointing to a plasmatocyte cluster with a gene expression profile associated
221 with mobility and migration. Among all plasmatocyte clusters, we found cluster C6 which presented a
222 strong immune activation phenotype with induction of *Jak/STAT* target genes including *Fasciclin 3*
223 (*Fas3*) and *Turandot-M* (*TotM*) among its TOP20 DE genes*,* but also activation of oxidative stress
224 response genes such as the heat shock proteins *Hsp23*, *Hsp26* and *Hsp27* or cytoskeletal genes
225 including *myosin Myo31DF* or *spire* (*spir*) (Figure 2E).

226 Due to the partially shared expression profile of genes across hemocyte clusters, we wondered if there
227 were genes exclusively expressed in individual clusters. However, cluster C1 showed that *Sema2a*
228 seems to be exceptionally high expressed in these homeostatic plasmatocytes and genes associated
229 with metabolic regulation (e.g. *InR*, *Lpin* or *bmm*) or Jak/STAT activation (e.g. *Fas3*), as seen in PQ-
230 associated clusters, are downregulated (Figure 2F). Cluster C5 showed enrichment for genes such as
231 the transcription factor *grainy head* (*grh*) but also cytoskeletal-associated genes such as *jitterbug* (*jbug*)
232 and *form3,* suggesting a migratory potential of plasmatocytes from this cluster within their host tissues
233 (Figure 2F). Interestingly, plasmatocyte cluster C6 presented with the most profound gene expression
234 changes compared to all other clusters. Similar to our previous observations, we identified that genes
235 specifically expressed in this cluster were associated with Jak/STAT pathway activation (e.g. *Fas3*,
236 *TotM*), cytoskeletal rearrangements and migration (e.g. *Myo31DF*, *spir* or *cheerio* (*cher*)) and response
237 to oxidative stress (e.g. *Nicotinamide amidase* (*Naam*) or *Hsp23*) (Figure 2F). We also included the
238 crystal cell cluster C8 in this analysis and verified unique expression of crystal cell markers compared
239 to the seven plasmatocyte clusters (Figure 2F). Our snRNA-seq analysis revealed that adult hemocytes
240 respond differentially to oxidative stress with a specific cluster of plasmatocytes associated with
241 immune activation and stress response. Despite our findings that on systemic level we did not detect

242 a strong induction of immune activation upon oxidative stress, we now provide evidence that
243 plasmatocyte cluster C6 showed a substantial immune response towards oxidative stress.

244 **Direct response to oxidative stress *in vitro* mimics the transcriptional changes seen in cluster C6**
245 **plasmatocytes *in vivo*.**

246 Plasmatocytes responded to PQ-mediated oxidative stress in different cellular states. We defined
247 cluster C6 as a cell state which is associated with oxidative stress response and immune activation.
248 Since cluster C6 showed gene expression associated with oxidative stress and immune activation we
249 focused our further analysis on this cluster. To further substantiate our findings and address the
250 signaling pathways that could lead to diverse transcriptional states, we inferred the transcription factor
251 (TF) network based on gene expression data (Figure 3A). This analysis revealed that genes with binding
252 sites for *Xbp1* were enriched. *Xbp1* is a transcription factor associated with stress response. In addition
253 to this, the Nf-κB-related transcription factor *Relish* (*Rel*) and *kayak* (*kay*), a component of the *activator*
254 *protein-1* (*AP-1*) transcription factor complex induced by JNK signaling, were also enriched in this
255 cluster (Figure 3A). To determine if the gene expression signature of cluster C6 plasmatocytes reflects
256 a functional state of plasmatocytes directly induced by oxidative stress, we treated S2 cells, a
257 *Drosophila* plasmatocyte cell line, with different concentrations of PQ (15mM and 30mM) *in vitro*
258 (Figure S5). First, we performed flow cytometric analysis of ROS levels via CellROX staining after 6 and
259 24 hours PQ treatment compared to controls (Figure S5A-B). We observed a dose-dependent increase
260 in intracellular ROS at all time points analyzed with higher ROS levels at 6 hrs (0mM: 1903±64 median
261 fluorescence intensity (MFI), 15mM: 6735±1096 MFI, and 30mM: 7435±237 MFI) compared to 24 hrs
262 (0mM: 1236±135 MFI, 15mM: 4456±228 MFI, and 30mM: 5557±303 MFI) (Figure S5C). Increase in ROS
263 and oxidative stress can lead to cellular damage such as damage in nuclear and mitochondrial DNA.

264 We next tested if plasmatocytes directly exposed to oxidative stress might also experience this type of
265 stress response by performing comet assays of treated and untreated S2 cells. Upon PQ treatment, S2
266 cells showed a remarkable and dose-dependent increase in DNA damage compared to untreated cells
267 (0mM: 101.0±2.1, 5mM: 117.6±3.3, 10mM: 136.6±3.8, and 15mM: 147.8±5.5, data shown as olive tail
268 moment) (Figure S5D). We were then wondering if PQ-treated S2 cells would resemble cluster C6
269 plasmatocytes *in vivo* and performed gene expression analysis of S2 cells treated with 15mM PQ after
270 6 and 24 hrs. Comparable to our results for cluster C6 *in vivo*, we found a profound induction of the
271 Jak/STAT target genes by qRT-PCR. In S2 cells, we also detected a significant increase of the Jak/STAT
272 cytokines *upd1*, *upd2* and *upd3* (Figure S5E), which we did not see before *in vivo*. Furthermore, we
273 detected an increased expression of the JNK-target gene *puckered* (*puc*), but barely any induction of
274 metabolic genes (Figure S5E). All these results further support our hypothesis that direct exposure of

275 S2 cells with PQ *in vitro* mimics gene expression changes seen in a particular activated cell stage of
276 plasmatocytes upon oxidative stress *in vivo*.

277 Because we found enrichment of genes associated with the Nf-κB-related transcription factor *Rel* in
278 the immune-activated plasmatocyte cluster C6, we further verified if any other cytokines or AMPs are
279 induced in PQ-treated S2 cells. We identified a slight but significant induction of the cytokine *daw*, but
280 no other alterations in *dpp* or the AMPs *Drs*, *Dro* or *Mtk* (Figure S5F). The profound induction of
281 Jak/STAT target genes together with the activation of JNK target genes and oxidative stress induced
282 DNA damage in S2 cells *in vitro* highly support our hypothesis that cluster C6 plasmatocytes reflect a
283 cellular state associated with the direct response to oxidative stress *in vivo*. Along this line, we went
284 back to our snRNA-seq data and specifically searched for Jak/STAT target genes (*upd3*, *Socs36E*, *TotA*,
285 *TotM* and *Fas3*) across all clusters (Figure 3B). Here we identified an enriched expression of these genes
286 in cluster C6, and a unique expression of the pro-inflammatory cytokine *upd3* in cluster C6 which was
287 not detected in any other hemocyte cluster (Figure 3B). Of note, we did not detect elevated *upd3* levels
288 in gene expression profiling of whole flies (Figure 1B), but now unraveled elevated *upd3* induction in
289 the particular hemocyte cell cluster C6 upon PQ treatment. Interestingly, we also identified that
290 *Growth arrest and DNA damage-inducible 45* (*Gadd45*), a gene linking DNA damage signaling and stress
291 induced JNK signaling, was enriched in plasmatocyte cluster C6 (Figure 3B). This could indicate that
292 plasmatocytes within cluster C6 undergo oxidative stress mediated DNA damage, which results in
293 activation of the DNA damage repair machinery but also JNK activation, similar to what we have seen
294 in S2 cells *in vitro*. However within our snRNA-seq analysis, the JNK target gene *puc* was expressed
295 across all hemocyte clusters analyzed *in vivo* without a specific induction in cluster C6 (Figure 3B). We
296 looked again into the expression of metabolic genes including *Thor* and *InR* as well as other cytokines
297 such as *dpp*, *daw* or *egr* but could not detect a specific enrichment in cluster C6 similar to our results
298 from PQ-treated S2 cells *in vitro* (Figure 3B). These findings from the snRNA-seq analysis *in vivo* and S2
299 cells *in vitro* support the hypothesis that cluster C6 plasmatocytes represent a functional state of
300 activated plasmatocytes directly responding to oxidative stress by JNK signaling and Jak/STAT pathway
301 activation. Furthermore, we found evidence that cluster C6 specifically expresses the cytokine *upd3*,
302 which could reflect an important mediator for oxidative stress response.

303 **Oxidative stress induces distinct cell states in the fat body, including the induction of a Jak/STAT**
304 **responsive and the loss of an AMP-producing cell cluster.**

305 The diversification of plasmatocytes during oxidative stress and the defined cytokine producing
306 immune-activated cell cluster C6 could play a key role in immune response to oxidative stress and also
307 for interorgan communication. To further explore this hypothesis, we aimed to gain further insights
308 into single-cell transcriptomic profiles of the *Drosophila* fat body during oxidative stress. Using cell

309 type-specific signatures, three of the clusters were annotated as fat body cells (clusters: 1, 3 and 4)
310 (Figure 2A-B). Re-scaling and clustering of all 3150 identified fat body nuclei revealed 8 distinct clusters
311 (Figure 4A). First, we verified fat body-specific signature gene expression across these clusters (Figure
312 S4B) and excluded expression of hemocyte-specific signature genes (Figure S4C). From the eight
313 distinct fat body cell clusters, we identified that cluster C1, C6 and C8 were mainly enriched with cells
314 obtained from control flies, whereas clusters C2-5 were almost exclusively derived from PQ treated
315 flies (Figure 4B, Figure S4D). Only cluster C7 represents cells from both conditions (Figure 4B, Figure
316 S4D). To define the transcriptional changes between these eight fat body cell clusters, we analyzed the
317 TOP20 DE genes across all fat body cell clusters (Figure 4C, Table S2), as well as the unique regulated
318 genes in each specific cluster compared to all others (Figure 4D). Here the cluster C1, mostly derived
319 of fat body cells from control flies, showed an enrichment for gene induction associated with
320 triglyceride storage, such as *Fatty acid synthase 1* (*FASN1*), *Glycerol-3-phosphate dehydrogenase 1*
321 (*Gpdh1*) or *Acyl-CoA synthetase long-chain* (*Acsl*), as well as fat body signature genes (Figure 4C-D).
322 Interestingly cluster C8, which mostly consisted of cells from control food, showed a distinct expression
323 of AMP genes including *Dro*, *Drs* or *Diptericin-B* (*DptB*), however this cluster completely disappeared
324 after PQ feeding (Figure 4C-D). In contrast, PQ treatment induced several fat body specific cell clusters
325 which were not found in control conditions. For example, cluster C2, C4 and C5, which showed a strong
326 gene induction of oxidative stress response genes, but also genes associated with Jak/STAT pathway
327 (e.g. *Socs36E*, *upd3*, *Fas3*, *TotA*) and JNK activation (e.g. *puc*, *kay*) (Figure 4C-D). In all of these clusters,
328 genes associated with triglyceride storage were significantly reduced. This is in line with our findings
329 showing a reduction in triglyceride storage in the fat body upon oxidative stress (Figure 1F, Figure S1E-
330 F). Overall our data revealed that the fat body has a unique heterogeneity upon oxidative stress with
331 a clear separation of clusters with JNK and Jak/STAT activation signature, which could be either
332 activated by the PQ-induced oxidative stress itself or by the cytokines released by immune-activated
333 hemocytes, especially *upd3*.

334 **Loss of DNA damage signaling in adult hemocytes results in elevated *upd3* levels and a decreased**
335 **survival on oxidative stress**

336 To evaluate the role of immune activation in hemocytes during oxidative stress response, we aimed to
337 specifically explore the implication of DNA damage signaling in hemocytes (Figure 1-3). Previously it
338 has been observed that oxidative stress-induced DNA damage supports immune activation in
339 macrophages via DNA damage signaling[27]. Based on our findings, we predict that also in adult
340 hemocytes oxidative stress not only drives genome instability and activates repair, but plays a role in
341 the induction and modulation of immune activation via specific gene expression changes in cluster C6
342 plasmatocytes. To test if DNA damage signaling is involved in the response of adult hemocytes to
343 oxidative stress, we analyzed flies with a hemocyte-specific knock-down for different genes of the DNA

damage repair (DDR) machinery including the DNA damage sensing kinases *telomere fusion* (*tefu*) and *meiotic 41* (*mei-41*) and the MRN complex protein *nbs*. Of note, by targeting adult hemocytes, mostly plasmatocytes are targeted which make up 95% of all hemocytes in the adult fly.

We generated *Hml>mei-41-IR* (*w;Hml-Gal4,UAS-2xeGFP/UAS-mei-41-IR*), *Hml>tefu-IR* (*w;Hml-Gal4,UAS-2xeGFP/UAS-tefu-IR*), *Hml>mei41-IR;tefu-IR* (*w;Hml-Gal4,UAS-2xeGFP/UAS-mei-41-IR;UAS-tefu-IR*) and *Hml>nbs-IR* (*w;Hml-Gal4,UAS-2xeGFP/UAS-nbs-IR*) flies (Figure S6A). First, we compared their susceptibility to PQ treatment after 18 hrs and found significantly increased susceptibility to the treatment across all DDR-deficient lines compared to the control genotype (*Hml/+*: 10.7±1.2%, *Hml>mei-41-IR*: 40.7±4.8%, *Hml>tefu-IR*: 20.7±4.3%, *Hml>mei41-IR;tefu-IR*: 37.5±4.8% and *Hml>nbs-IR*: 48.2±6.7%) (Figure 5A). In these flies, decreased survival after PQ did not correlate to an overall reduction in lifespan on normal food and a decrease in fitness (Figure S6B).

Next, we inquired if DDR-deficiency in hemocytes might increase susceptibility of the fly to other stresses. For this we challenged all genotypes with starvation. Importantly, we did not observe a decreased survival of DDR-deficient flies on starvation compared to the control genotype, indicating that the observed susceptibility to oxidative stress of flies with a DDR-deficiency in hemocytes is specifically caused by oxidative stress due to PQ treatment (Figure S6C). As defects in the DDR machinery in hemocytes might already affect the development during embryonic and larval stages, we used a hemocyte-specific temperature-inducible knock-down of *mei-41*, *tefu* and *nbs1* which was induced by a temperature shift to 29°C directly after eclosion from the pupae to induce a knockdown in adult hemocytes only. We analyzed the lifespan of *Hml-Gal80^{ts}>mei-41-IR* (*w;Hml-Gal4,UAS-2xeGFP/UAS-mei-41-IR;tub-Gal80*), *Hml-Gal80^{ts}>tefu-IR* (*w;Hml-Gal4,UAS-2xeGFP/UAS-tefu-IR;tub-Gal80*), *Hml-Gal80^{ts}>mei-41-IR;tefu-IR* (*w;Hml-Gal4,UAS-2xeGFP/UAS-mei-41-IR;tub-Gal80/UAS-tefu-IR*) and *Hml-Gal80^{ts}>nbs-IR* (*w;Hml-Gal4,UAS-2xeGFP/UAS-nbs-IR;tub-Gal80*) compared to control flies *Hml-Gal80^{ts}/+* (*w;Hml-Gal4,UAS-2xeGFP/+;tub-Gal80*) and again found no alterations in overall lifespan of all genotypes analyzed on control food except a slight decrease in lifespan of *Hml-Gal80^{ts}>mei-41-IR;tefu-IR.* (Figure S6D). In contrast, we again found a higher susceptibility to oxidative stress via PQ-feeding in the DDR-deficient lines compared to control (*Hml-Gal80^{ts}/+*: 30.3±5.2%, *Hml-Gal80^{ts}>mei-41-IR*: 36.2±4.3%, *Hml-Gal80^{ts}>tefu-IR*: 52.4±6.9%, *Hml-Gal80^{ts}>mei-41-IR;tefu-IR*: 72.3±6.3% and *Hml Hml-Gal80^{ts}>nbs-IR*: 36.2±4.3%) (Figure S6E), which directly confirms our previous results and conclusions (Figure 5A).

As we have seen before that loss of hemocytes is detrimental for the survival on oxidative stress, we wanted to exclude a reduction in hemocytes in the DDR deficient fly lines as a cause of the higher susceptibility to oxidative stress. We quantified GFP^{+} hemocytes in *Hml>mei-41-IR*, *Hml>tefu-IR*, *Hml>mei-41-IR;tefu-IR* and *Hml>nbs-IR* flies (Figure 5B, Figure S6A). We did not find alteration in

378 hemocyte number across all fly lines on control food (with the exception of an increase in hemocytes
379 in the *Hml>tefu-IR* line), nor did we observe any effect of PQ treatment on the number of hemocytes
380 in DDR-deficient flies (Figure 5B, Figure S6A).

381 Next, we analyzed if the loss of the DDR signaling machinery via knockdown of *tefu* and *mei41* results
382 in increased DNA damage in hemocytes. Comet assays of isolated hemocytes from DDR deficient flies
383 and the control genotype on PQ and control food only indicated a slight increase in DNA damage in
384 these flies, which demonstrates that the higher susceptibility of DDR deficient flies is not due to a loss
385 of hemocyte numbers or a substantial increase in DNA damage, but rather due to changes in the
386 downstream DDR-signaling events modulating immune activation of hemocytes (Figure 5C). Other
387 studies demonstrated that upon tissue damage JNK-mediated secretion of the JAK/STAT cytokines
388 upd1, upd2 and upd3 is a critical step for innate immune signaling[28,29]. Furthermore, DNA damage
389 signaling is essential to induce such an immune response and to regulate insulin signaling[30]. To
390 elucidate the implication of DDR signaling on hemocyte activation and oxidative stress resistance, we
391 measured the gene expression levels of *upd* cytokines as well as JNK and Jak/STAT targets in DDR
392 deficient flies and controls on PQ and control food. Loss of DNA damage signaling in hemocytes
393 induced a significant induction of *upd3* expression upon PQ treatment in *Hml>tefu-IR* and *Hml>mei-*
394 *41-IR;tefu-IR* flies (Figure 5D). In contrary, *upd1* and *upd2* were not significantly changed in DDR-
395 deficient flies (Figure 5D). We measured the Jak/STAT target genes *Socs36E* and *TotA* on systemic level.
396 A slight induction of *Socs36E* expression in all DDR-deficient genotypes on PQ, but only *Hml>mei-41-*
397 *IR;tefu-IR* flies showed a significant induction of *Socs36E* upon PQ treatment compared to control food
398 and *Hml/+* flies on PQ (Figure 5D). *TotA* expression tended to be reduced upon PQ treatment across
399 all genotypes analyzed. However, when we checked the levels of *puc* as a *JNK signaling* target gene,
400 we found a significant induction on PQ treatment in *Hml>tefu-IR*, *Hml>mei-41-IR;tefu-IR* and *Hml>nbs-*
401 *IR* flies, which was not seen in control flies upon PQ treatment (Figure 5D). When we analyzed the gene
402 expression of genes involved in metabolism and energy mobilization, we detected a significant
403 induction and dysregulation of *Thor* and *InR* in all DDR-deficient genotypes upon PQ treatment
404 compared to control flies (Figure 5E), as well as a slight induction of *Pepck1* (Figure 5E). To exclude that
405 these changes in energy mobilization are due to altered expression of *Ilps*, we analyzed the levels of
406 *Ilp*2, *Ilp3* and *Ilp5* in all genotypes on control and PQ-food, but could not detect remarkable alterations
407 here (Figure 5E). To further exclude that the higher susceptibility of DDR-deficient flies and seen
408 alterations in stress response are due to inefficient mobilization of triglycerides, we measured stored
409 triglycerides across all genotypes and found efficient mobilization of triglyceride storage upon PQ
410 treatment in all genotypes compared to control food (Figure 5F).

411 From our results we can conclude that DNA damage signaling in adult hemocytes, mostly consisting of
412 plasmatocytes, essentially determines susceptibility to oxidative stress. Loss of DNA damage signaling
413 in hemocytes results in upregulation of *JNK* signaling and elevated expression of the pro-inflammatory
414 cytokine *upd3*, as well as transcriptional alterations in energy mobilization and insulin signaling. Based
415 on our previous results on the role of hemocytes during oxidative stress, we can therefore assume that
416 the DNA damage signaling machinery in hemocytes is activated by oxidative stress and plays an
417 essential modulatory and rate-limiting role for subsequent immune activation.
418
419 **Adult hemocytes control susceptibility to oxidative stress by JNK signaling and *upd3* release**
420 To this point, our data suggests that oxidative stress-induced DNA damage signaling in hemocytes
421 limits immune activation and stress response upon oxidative stress. As we found that increased *upd3*
422 levels correlate with a higher susceptibility to oxidative stress of flies with DDR-deficient hemocytes,
423 we aimed to test if hemocyte-derived *upd3* is a major source to regulate susceptibility to PQ-induced
424 oxidative stress. To do so, we either over-expressed *upd3* in hemocytes in *Hml>upd3* (*w;Hml-Gal4,UAS-*
425 *2xeGFP/UAS-upd3*) flies or performed a hemocyte-specific knockdown of *upd3* in *Hml>upd3-IR* (*w;Hml-*
426 *Gal4,UAS-2xeGFP/UAS-upd3-IR*) flies (Figure S6F). Both genotypes showed a normal overall lifespan
427 compared to the *Hml/+* control (Figure S6G), but when we compared their susceptibility to PQ-induced
428 oxidative stress, *Hml>upd3* flies showed a drastically decreased survival on PQ, whereas *Hml>upd3-IR*
429 flies did not show a changed survival on PQ treatment after 18 hours (Figure 6A). We tested *upd3*
430 expression levels on a whole fly level and found a slight but not significant induction in *Hml/+* flies after
431 PQ treatment compared to control food, in line with our previous results (Figure 1B and 6B). As
432 expected, *Hml>upd3* flies showed increased levels of *upd3* in both treatment groups compared to the
433 other genotypes, but also showed a significant increase of *upd3* upon PQ compared to control food
434 (Figure 6B). Surprisingly, *Hml>upd3-IR* flies still showed a slight induction of *upd3* upon PQ treatment,
435 which could potentially be derived from another cellular source after eliminating hemocyte-derived
436 *upd3*, for example fat body cells, as seen in our snRNA-seq analysis.
437 To identify if the higher susceptibility of *Hml>upd3* flies to oxidative stress was due to reduced
438 hemocyte numbers, we quantified hemocytes across all three genotypes, but did not see any
439 significant changes of hemocyte number in both genotypes compared to *Hml/+* control flies on control
440 food and PQ (Figure 6C and Figure S6F). Only in the *Hml>upd3-IR* flies we found a reduction of
441 hemocytes between flies on control food and PQ, but without consequences for their susceptibility to
442 oxidative stress (Figure 6C and Figure S6G). Our data indicate that elevation of hemocyte-derived *upd3*
443 is sufficient to increase the mortality of adult flies on PQ-mediated oxidative stress. Yet we could not
444 exclude other cellular sources than hemocytes for *upd3* upon oxidative stress. Therefore, we wanted
445 to probe if hemocyte-derived *upd3* is sufficient to increase the susceptibility to PQ treatment in the

446 absence of other cellular sources. We backcrossed *Hml>upd3* flies to *upd3*-null mutants (*upd3*^{null}) to
447 generate *upd3*^{null}*;Hml>upd3* flies (*upd3*^{null}*;Hml-Gal4,UAS-2xeGFP/UAS-upd3)* and compared their
448 survival on PQ to *Hml/+* and *upd3*^{null} flies (Figure 6D). Of note, we found that *upd3*^{null} mutants had a
449 significant reduced susceptibility to oxidative stress compared to *Hml/+* flies, however we found a
450 decreased survival in *upd3*^{null}*;Hml>upd3* flies when hemocytes alone overexpressing *upd3* similar to
451 the higher susceptibility of *Hml>upd3* flies (Figure 6D). We then wanted to test if loss of *upd3* would
452 also rescue the higher susceptibility of flies with DDR-deficient hemocytes and backcrossed
453 *Hml>mei41-IR;tefu-IR* to *upd3*^{null} flies to generate *upd3*^{null}*;Hml>mei41-IR;tefu-IR* flies (*upd3*^{null}*;Hml-*
454 *Gal4,UAS-2xeGFP/UAS-mei41-IR;UAS-tefu-IR*) (Figure 6D). Indeed we found a substantially decreased
455 susceptibility of these flies to oxidative stress compared to *Hml>mei41-IR;tefu-IR* flies, supporting our
456 hypothesis that loss of DNA damage signaling in hemocytes and subsequently increased levels of upd3
457 render adult flies more susceptible to oxidative stress.

458 Previous studies highlighted that JNK signaling can induce *upd3* expression in hemocytes[12]. In line with
459 these reports, we found enrichment of genes with *kayak/AP-1* binding motifs in the plasmatocyte
460 subset C6 which showed further upregulation of Jak/STAT target genes and also *upd3* expression
461 (Figure 3). Therefore, we wanted to verify if *JNK* activation in hemocytes acts as a direct downstream
462 signal activated by oxidative stress and subsequently induces the release of the pro-inflammatory
463 cytokine *upd3*. We either overexpressed a constitutive active form of *JNKK hemipterous* (*hep*) in
464 hemocytes using *Hml>hep[act]* (*w;Hml-Gal4,UAS-2xeGFP/UAS-hep[act]*) flies or overexpressed a
465 dominant-negative version of the Jun kinase *basket* (*bsk*) in hemocytes using *Hml>bsk-DN* (*w;Hml-*
466 *Gal4,UAS-2xeGFP/UAS-bsk-DN*). We compared their survival on PQ after 18 hrs and in line with our
467 previous results, we found an increased susceptibility of *Hml>hep[act*] flies to PQ treatment, but not
468 of *Hml>bsk-DN* flies compared to the control genotype (Figure 6E). We again analyzed the overall
469 lifespan of these flies on normal food and could not find differences between the genotypes (Figure
470 S6H). Furthermore, when we analyzed *upd3* expression in these flies upon PQ treatment, we found a
471 significant induction of *upd3* expression after PQ treatment in *Hml>hep[act*] compared to control food,
472 but only a slight increase in *Hml/+* and *Hml>bsk-DN* flies upon PQ feeding (Figure 6F). These findings
473 support a substantial role of JNK-mediated induction of *upd3* in hemocytes upon oxidative stress.

474 In summary, our study revealed a defined immune-responsive subset of plasmatocytes during
475 oxidative stress. We show that this oxidative stress-mediated immune activation seems to be
476 regulated by DNA damage signaling in hemocytes, which controls JNK activation and subsequent *upd3*
477 expression. Loss of DNA damage signaling and over-induction of JNK signaling or upd3 in hemocytes
478 release renders the adult fly more susceptible to oxidative stress.

479

480 **Discussion**

481 Similar to vertebrate macrophages, oxidative stress triggers immune activation in *Drosophila*
482 hemocytes[18]. However, this immune activation was not obvious on a systemic level upon PQ-mediated
483 oxidative stress. In contrast, localized oxidative stress-induced immune activation in damaged tissues
484 is an essential step of the *Drosophila* immune response to infection or injury[19,31]. However, the precise
485 contribution of *Drosophila* macrophages in this immune activation, in the organ-to-organ
486 communication during stress response and the implication in the organism's survival upon increased
487 oxidative stress remained so far ill-defined. Overall, we describe the induction of diverse cellular states
488 of adult hemocytes, namely plasmatocytes, during oxidative stress with a particular subset of
489 plasmatocytes (cluster C6) which directly responds to oxidative stress by immune activation. We
490 demonstrated that this immune activation seems to be at least partially controlled by the DNA damage
491 signaling machinery in hemocytes. Loss of *nbs*, *tefu* or *mei-41* in hemocytes renders the organism more
492 susceptible to oxidative stress without significantly affecting oxidative stress mediated DNA damage,
493 but with an enhanced induction of JAK/STAT and JNK signaling, accompanied by changes in genes
494 associated with energy mobilization and storage. In line with that, we describe substantial changes in
495 the fat body on the transcriptomic level with diverse cell states, indicating decrease of triglyceride
496 storage and induced response to oxidative stress and immune activation, but loss of AMP-producing
497 cells. Finally, we showed that the control of hemocyte-derived *upd3* is key for the survival of the
498 organism upon oxidative stress and that induction of the *JNK/upd3* signaling axis in hemocytes is
499 sufficient to increase the susceptibility to oxidative stress. Hence, we postulate that hemocyte-derived
500 *upd3* is most likely released by the activated plasmatocyte cluster C6 during oxidative stress *in vivo*
501 and is subsequently controlling energy mobilization and subsequent tissue wasting upon oxidative
502 stress.

503

504 *Drosophila* hemocytes have been described before to react to PQ-mediated or infection-mediated
505 intestinal damage via release of cytokines to promote ISC proliferation in the gut[14,17]. PQ is a widely
506 used model in *Drosophila* to induce oxidative stress via oral uptake[32]. In many reports the gut has been
507 described to be the most affected organ and ISC proliferation is an essential step to regenerate the
508 injured intestinal epithelium[33,34]. PQ treatment has been described to cause gut leakage and therefore
509 this could be a potential cause of death for the fly[14], though we did not find signs of gut leakage within
510 the 18 hours PQ treatment with a concentration of 15mM. Aside from the gut, oral PQ treatment was
511 shown to induce oxidative stress in many organs including hemocytes[35], oenocytes[36] and the brain[37],
512 indicating that the induced oxidative stress is not only localized to the gut tissue. PQ-induced oxidative
513 stress was described before to cause neurodegeneration with parkinsonism-like symptoms,
514 accompanied by strong immune activation and upregulation of *JNK* signaling in the CNS[37], an activation

515 profile similar to the identified activated plasmatocyte cluster C6 and the activated fat body clusters
516 C2 and C4 in our snRNA-seq analysis. The snRNA-seq analysis further revealed distinct hemocyte
517 clusters with seven plasmatocyte clusters and one crystal cell cluster. Whereas the plasmatocyte
518 clusters C1 and C7 seem to represent cellular states found in steady state conditions only, we identified
519 several other clusters which seemed to be exclusive or at least enriched under PQ treatment.
520 Interestingly, we only identified one cluster, C6, which specifically responded to oxidative stress via
521 immune activation and upregulation of oxidative stress response genes but also *Jak/STAT* and *JNK*
522 target genes. We postulate that these cells might be directly exposed to the oxidative stress because
523 their signature resembles the one of S2 cells directly treated with PQ *in vitro*. Even though oxidative
524 DNA damage in hemocytes was followed by immune activation *in vitro* and *in vivo*, it remains to be
525 determined if this activation is induced by cytokines derived from damaged organs during oxidative
526 stress or by the oxidative stress directly. The hypothesis that this cluster is directly exposed to oxidative
527 stress is further supported by an upregulation of genes such as *Hsps* in this cluster which are known to
528 be directly induced by oxidative stress[38]. Furthermore, we found evidence that oxidative DNA damage
529 and induced DNA damage signaling dynamically modulate immune activation cascades in cluster C6
530 plasmatocytes. This was supported by the increased DNA damage in S2 cells by PQ treatment but also
531 the enrichment of DDR-associated genes such as *Gadd45* in cluster C6, which is associated with *JNK*
532 activation and is further implicated in oxidative stress induced DNA damage[37]. Constant DNA damage
533 signaling and repair is an essential step in all tissues to maintain tissue homeostasis[39].

534 In our study, we point to a potential role of DNA damage signaling as a rate-limiting step for immune
535 activation and response to oxidative stress in hemocytes. We did not find indications of canonical DNA
536 damage response, such as induced apoptosis in hemocytes due to the oxidative DNA damage. Non-
537 canonical DNA damage sensing has been implicated in immune responses in vertebrates and
538 invertebrates[30,37,40,41]. It was demonstrated that vertebrate macrophages *in vitro* respond similarly to
539 immune stimuli such as infection by synergistic activation of DDR and type I interferon signaling to
540 induce downstream immune signaling cascades[27]. Here, we provide new evidence in *Drosophila* that
541 potentially non-canonical DNA damage is used by immune cells *in vivo* to modulate and especially
542 control their immune response including pro-inflammatory cytokine release upon oxidative stress.
543 Localized DNA damage in larval epithelial cells has been shown to induce non-canonical DNA damage
544 activity leading to the secretion of *upds* and the regulation of hemocyte expansion and activation, as
545 well as subsequent hemocyte-mediated regulation of energy storage in the fat body[30]. In further
546 support of our results, one report previously demonstrated that loss of DNA damage signaling
547 machinery induced the release of *upd3* in hemocytes[14]. Most likely, the identified plasmatocyte cluster
548 C6 is a central cellular source of this signal. However, we also detected *upd3* induction in the PQ-
549 induced fat body cell cluster C4 as potential secondary source of upd3, which needs to be further

550 determined in future studies. Furthermore, anatomical localization of this upd3-producing
551 plasmatocyte cluster, as well as spatial distribution and cross-talk of the different plasmatocyte and
552 fat body cell clusters would be of interest. We describe a strong connection between the control of
553 *upd3* expression by hemocytes and the susceptibility of the adult fly to oxidative stress. Upon oxidative
554 stress, we observe decreased triglycerides and glycogen stores and altered gene expression such as
555 induced expression of lipolytic enzymes and other *foxo* target genes indicating energy mobilization
556 from the adult fat body, which was further supported by the transcriptomic profiling of fat body cells.
557 Accumulating evidence throughout our study points to an implication of hemocyte-derived *upd3* in the
558 control of energy mobilization and tissue wasting during oxidative stress. Our data from hemocyte-
559 deficient flies indicating defects in energy mobilization and maintenance of free glucose levels further
560 support this assumption. Our presented findings are in line with our previous studies where we showed
561 that upon high fat diet hemocytes produce high levels of *upd3* which induces insulin insensitivity in
562 many tissues by activating *Jak/STAT signaling* in these organs and inhibiting the insulin signaling
563 pathway[12]. Furthermore, we and others described a central role for hemocyte derived *upds* in the
564 control of glucose metabolism in muscles during steady state and upon infection[13,42]. As shown before,
565 hemocytes produce high levels of *upd3* upon infection with *Mycobacterium marinum* which also
566 caused tissue wasting and extensive energy mobilization in a *foxo*-dependent manner[11,43].

567 Our study provides further evidence that hemocytes serve as essential signaling hubs in "organ to
568 organ communication" during oxidative stress, which is in line with previous studies in immune
569 challenge as well as steady state[19,42,44]. Our findings in *Drosophila* highlight the role of macrophages
570 for the survival on oxidative stress with an urgent need for a balanced immune response to overcome
571 the tissue damage. We further unravel the diverse responses of hemocytes and fat body cells towards
572 oxidative stress which can now serve as a baseline to further explore the spatiotemporal
573 macrophage/hemocyte responses to oxidative stress and their communication with other host tissue
574 cells such as the fat body. Future in depth analysis of the regulation of these cellular states and their
575 coupling to tissue repair will allow to gain new insights for the treatment of diseases where tissue
576 repair and tissue wasting needs to be balanced, including cancer or neurodegenerative diseases.
577

578 **Acknowledgements and Funding**

579 The authors are very grateful to the members of the Kierdorf lab for their help and support. The
580 authors would especially like to thank M. Oberle for her exceptional help with the maintenance of the
581 Drosophila stocks and the management of the fly room. We would like to acknowledge the Lighthouse
582 Core Facility and its staff, especially J. Bodinek-Wersing and U. Jagadeshwaran, for their assistance with
583 the sorting of nuclei. The authors are especially grateful to D. Ganser and H. Fischer for the continuous
584 support throughout the study. Graphical abstract was created with BioRender.com. KK was supported

585 by project grants of the Fritz Thyssen Foundation and of the German Research Foundation (DFG). MSD
586 was supported by Wellcome Trust (207467/Z/17/Z) and Biotechnology and Biological Sciences
587 Research Council (BBSRC) (BB/W/001004/1). KK, MP, and OG were supported by the DFG through
588 project grants within SFB/TRR167 (Project ID 259373024) and by project grants within CRC1479
589 (Project ID 441891347). KK, MP, OG, and AC were supported by the DFG under Germany's Excellence
590 Strategy (grant no. CIBSS—EXC-2189, Project ID 390939984). AC was further supported by the
591 Boehringer Ingelheim Foundation (Plus3 Programme). OG was further supported by the European
592 Research Council (ERC) through Starting Grant 337689 and Proof-of-Concept Grant 966687, and by the
593 DFG through project grants in GRK2606 (Project ID 423813989), SFB1425 (Project ID 422681845), and
594 SFB1160 (Project ID 256073931), as well as by the EU-H2020-MSCA-COFUND EURIdoc programme (No.
595 101034170). MP was further supported by the Novo Nordisk Foundation, the Ernst Jung Foundation,
596 the DFG through project grants in SFB992 (Project ID 192904750), and SFB1160 (Project ID
597 256073931), a Reinhart Koselleck grant and the Gottfried Wilhelm Leibniz prize, the Ministry of
598 Science, Research and Arts of the state of Baden-Wuerttemberg (Sonderlinie 'Neuroinflammation')
599 and by the Alzheimer Forschung Initiative e.V. (AFI). GM was supported by a Marie Skłodowska-Curie
600 postdoctoral fellowship.
601
602 **Author Contributions**

603 FH contributed to project planning, performed all experiments, analyzed data, edited the manuscript
604 and prepared the figures. TM and PW performed experiments, helped with the data analysis, and
605 edited the manuscript. CC performed the snRNA-seq experiment and bioinformatics analysis of the
606 hemocytes. GM performed data preprocessing and supported bioinformatics analysis. AC, MSD, KP,
607 OG, and MP provided equipment and reagents, helped to analyze and interpret data, and edited the
608 manuscript. KK planned and supervised the project, conceptualized the study and wrote the
609 manuscript.

610 **Competing Interests Statement**

611 The authors declare no competing financial or scientific interests.

612 **Methods Section**

613 *Drosophila melanogaster stocks:*

614 Flies were reared on a high yeast food containing 10% brewer's yeast, 8% fructose, 2% polenta and
615 0.8% Agar. Propionic acid and nipagin were added to prevent bacterial or fungal growth. All crosses
616 (except those containing the *tub-Gal80^{ts}* construct or otherwise noted) were performed at 25°C with
617 a 12 hours dark/light cycle. The crosses with *tub-Gal80^{ts}* were performed at 18°C to ensure the
618 inhibition of the Gal4-protein during developmental stages of the fly. The experimental male F1 flies

619 were transferred to 29°C as soon as they hatched and were aged for six days. All transgenic lines used
620 in this study are listed in the Table S3.

621 *Lifespan/Survival assays:*

622 Male flies were collected after eclosion and groups of 20 age-matched flies per genotype were housed
623 in a food vial. The survival experiments were performed at 29°C. The vials were placed horizontal to
624 avoid that flies fall into the food and become stuck. Dead flies were counted in a daily manner. The
625 flies were transferred into a fresh food vial twice per week without CO_2 anesthesia.

626 *Paraquat treatment:*

627 Flies were maintained at 29°C for six days prior to treatment. On day six they were starved for 6 hours.
628 A filter paper soaked in 5% sucrose solution with or without 15mM Paraquat (PQ, Methyl viologen
629 hydrate, Acros Organics) was added after starvation. Flies were fed for 18 hours on the PQ containing
630 food in groups of ten. The PQ treatment was performed at 29°C in the dark[20]. To assess the survival
631 rate the dead flies per vial were counted and the percentage was calculated. The living flies were
632 further analyzed in other assays used in this study.

633 *Starvation experiments:*

634 10-20 age-matched male flies were kept in a vial containing 1% agar supplemented with 2% 1xPBS. The
635 starvation experiments were performed at 25°C. Dead flies were counted every hour. Several
636 individual experiments were performed and started on different daytimes to exclude diurnal derived
637 artifacts. The data of the individual experiments were pooled and analyzed with GraphPad Prism 9.2.0.

638 *Paraffin sections and stainings:*

639 Anaesthetized flies were washed in 75% ethanol for 5-10 seconds and transferred into 4% PFA for 30
640 minutes at room temperature. The flies were washed for 1 hour in PBS on a shaker. Subsequently the
641 flies were transferred into tissue cassettes, dehydrated and embedded in paraffin. The flies were cut
642 in 7µm thick sections de-paraffinated and stained on slides with Hematoxylin-Gill (II) for five minutes.
643 Subsequently the sections were blued in running water for ten minutes. It followed a 0.5% Eosin
644 treatment for five minutes and a final ethanol treatment with increasing concentrations until 100%.
645 The sections were transferred into Xylol and finally covered with synthetic resin and a cover slip.

646 Cryo sections and Oil Red O staining:

647 Anaesthetized flies were washed in 75% ethanol for 5-10 seconds and transferred into 4% PFA for 30
648 minutes at room temperature. Subsequently, the flies were dehydrated for 1h at 37°C in 30% sucrose
649 solution. The dehydrated flies were placed in a Tissue-Tek cryo-mold and embedded in Tissue-Tek®
650 O.C.T.™ Compound. The cryo-mold was placed on dry-ice which was embedded in a 100% ethanol bath
651 until the whole block was completely frozen. The flies were cut in 10µm sections and stained on the
652 slide. The slides were put on RT and dried. Subsequently, they were submerged in Oil red O solution
653 for 30 minutes. The slides were rinsed two times in deionized water and subsequently stained for two
654 minutes with hematoxylin to stain the nuclei. Finally, the slides were washed with water for 5 minutes
655 and covered with a cover slip and glycerin.

656 *Semi-quantitative Real-Time PCR:*

657 Three flies were pooled and smashed in 100µl TRIzol to stabilize and isolate the RNA. Chloroform was
658 used to extract the RNA followed by an isopropanol precipitation step. The RNA was cleaned with 70%
659 ethanol and solubilized in water. A DNAse treatment was performed to digest potential genomic DNA
660 contaminations. The purified and DNAse treated RNA was written into cDNA using RevertAid Reverse
661 Transcriptase (Thermo Scientific) at 37°C for one hour. The reaction was stopped by incubating for 10
662 minutes at 70°C. The subsequent RTqPCR was done in SensiMix SYBR Green no-ROX (Meridian
663 Bioscience) and was performed on a LightCycler 480 (Roche). The qPCR cycling started with a 10-
664 minute 95°C step followed by 50 cycles with the following times and temperatures: 15s at 95°C, 15s at
665 60°C and 15s at 72°C. The gene expression levels were normalized to the value of the measured loading
666 control gene Rpl1.

667 *Confocal microscopy:*

668 The flies were anesthetized with CO2, glued on a cover slip and imaged immediately. Confocal
669 microscopy was done with a Leica SP8 microscope (Leica) and a 10x/NA0.4 Leica air objective. The
670 images were acquired in a resolution of 512x512 with a scan speed of 600 Hz. Z-Stacks with a step size
671 of 5µm and tile scans (2x2 or 2x3 images per fly) were acquired to quantify the hemocytes in whole
672 flies. The tiled images were merged with the LAS-X software (Leica) and maximum projections were
673 created using Fiji/ImageJ. The hemocytes were counted in the maximum projection images of whole
674 flies.

675 *Smurf Assay:*

676 Smurf assays were performed to check the feeding behavior as well as the gut integrity of 7 days old,
677 male flies upon PQ treatment. Brilliant Blue dye (FCF) was added into 5% sucrose solution in a
678 concentration of 1% (w/v). PQ was added in concentrations of 2mM, 15mM and 30mM. Control food
679 was 5% sucrose and 1% Brilliant Blue without PQ. The flies were fed with blue food according to the
680 PQ-treatment protocol, as described above. Flies were analyzed after 18h of feeding on brilliant-blue
681 food. Three kinds of flies were distinguished. Flies that did not eat at all were excluded. Flies with a
682 blue gut or crop were classified as “non-smurf”. Flies which turned completely blue or showed
683 distribution of blue dye outside the gut were classified as “smurf”.

684 *Thin Layer Chromatography (TLC):*

685 Each sample in the TLC analysis contains 10 flies of the respective genotype. The flies were starved for
686 one hour before they were anesthetized with CO2 and transferred into 100µl chloroform:methanol
687 (3:1) on ice. The flies were centrifuged for 5 minutes at 15,000g at 4°C and subsequently homogenized
688 with a pestle. The sample was centrifuged again with the same settings. Lard was dissolved in
689 chloroform:methanol (3:1) and served as triglyceride control (standard 1). Standard 1 was used to
690 produce a standard curve with decreasing triglyceride concentrations. The samples and the standard
691 curve were loaded on a glass silica gel plate (Millipore). The mobile phase in the TLC chamber was
692 made with hexane:diethylether (4:1). The plate was placed in the chamber until the solvent front
693 reached the upper end of the plate. The plate was taken out, air dried and stained with ceric
694 ammonium heptamolybdate (CAM). Subsequently the plate was incubated at 80°C for 2 hours to
695 visualize the stained triglyceride bands. Images were taken with a gel documentation system (gelONE).
696 Triglyceride density was measured and the concentrations were calculated according the pre-
697 determined concentrations of the standard curve. Image analysis and calculations were done using
698 ImageJ.

699 *Glucose Assay:*

700 Seven days old male flies were used for the analysis. They were treated for 18h with PQ or sucrose
701 respectively. Subsequently the flies were starved for one hour to bring all flies into the same metabolic
702 state. Three flies were pooled as one sample and manually homogenized in 75µl TE + 0.1% Triton X-
703 100 (Sigma Aldrich). The samples were incubated for 20min at 75°C to inactivate any intrinsic
704 enzymatic activity. 5µl of the samples were loaded into a flat-bottom 96-well plate. Each sample was
705 measured four times to measure glucose, trehalose, glycogen and the fly background respectively. The
706 fly background was determined by diluting the fly sample with water. Glucose reagent (Sentinel
707 Diagnostics) was added to the fly sample to measure the glucose levels. Trehalase (Sigma Aldrich) or
708 amyloglucosidase (Sigma Aldrich) was added to the glucose reagent to measure trehalose or glycogen
709 respectively. Plates were incubated for 24h at 37°C before the colorimetric measurement was
710 performed at a wavelength of 492nm on a Tecan® Spark plate reader. The concentrations were
711 calculated according to standards loaded on the same plate.

712 *Nuclei FACS sorting:*

713 100 male *Hml-dsRed.nuc* flies per sample were homogenized in 500µl ice-cold EZ nuclei lysis buffer
714 (Sigma). Another 500µl EZ lysis buffer was added and the nuclei were incubated for five minutes on
715 ice. Following a pre-filtration step with a 70µm cell strainer (Miltenyi filters) the nuclei were
716 centrifuged at 500g for six minutes at 4°C. The pellet was resuspended and incubated in 1ml of EZ lysis
717 buffer for five minutes on ice following a second centrifugation step with previous used settings. After
718 discarding the supernatant, 500µl of nuclei wash and resuspension buffer (1x PBS; 1% BSA; 0.2U/µl
719 RNase inhibitor, NEB) was added without resuspending the pellet and incubated for 5 minutes on ice.
720 Subsequently the pellet was resuspended with additional 500µl nuclei wash and resuspension buffer.
721 The nuclei were centrifuged using previous settings and subsequently washed with 1ml of nuclei wash
722 and resuspension buffer. After centrifugation the pellet was resuspended and incubated for 15
723 minutes with nuclei staining solution containing DAPI (1:1000) and DRAQ7 (1:100). The nuclei were
724 washed once with 1ml nuclei wash and resuspension buffer. After centrifugation the pellet was
725 dissolved in 200µl wash and resuspension buffer, filtered through a 40µm filter and sorted on a BD
726 FACS ARIAIII. A duplet exclusion was performed by gating on singlets in FSC-A vs. FSC-W plot.
727 Subsequently DRAQ7+DAPI+ events were sorted into nuclei wash and resuspension buffer.

728 *Single nucleus library preparation and sequencing:*

729 For single nucleus library preparation, nuclei were loaded onto a Chromium Single Cell 3' G Chip (10X
730 Genomics) to generate single-nucleus gel beads in emulsion (GEM) according to the manufacturer's
731 instructions without modifications using Chromium Next GEM Single Cell 3' Reagents Kit v3.1 (10X
732 Genomics). In order to multiplex the samples for sequencing, Single Index Kit T Set A (10x Genomics)
733 was used for library preparation according to the manufacturer's instructions. The cDNA content and
734 size of post-sample index PCR samples was analyzed using a 2100 BioAnalyzer (Agilent). Library
735 quantification was done using NEB Next® Library Quant Kit for Illumina® (New England Biolabs)
736 following manufacturer's instructions. Sequencing libraries were loaded on an Illumina Nextseq 550
737 flow cell, with sequencing settings according to the recommendations of 10× Genomics. Sample de-
738 multiplexing was done using built-in BCL2FASTQ. Cell Ranger v6 software was implemented for gene
739 alignment to the fly genome. The *Drosophila melanogaster* genome assembly and annotation file were
740 downloaded from Ensembl (Release 104). The annotation files were filtered as suggested by 10x
741 Genomics, to keep only the categories of interest (i.e. protein coding genes, long intergenic noncoding

742 RNAs, antisense, pseudogenes). Cell Ranger v6 with the "include-intron" parameter was used for the
743 generation of the count data.

744 *snRNA-seq data analysis*

745 Downstream analysis implemented the SoupX v1 and Seurat v4 R-based packages. The matrix for each
746 sample was loaded using the SoupX package[45] and ambient RNA contamination was calculated using
747 the default setting. The corrected matrix together with metadata on treatment were used to create an
748 object in Seurat v4[23]. Doublet detection was done using the DoubletFinder package v2[46]. After doublet
749 exclusion, a combined object was created from the list by using the "merge" function. Nuclei with <
750 5% of mitochondrial contamination and between 400 and 1,700 genes expressed were retained for
751 further analysis. The filtered raw count matrix was log-normalized within each nucleus. The top 3,000
752 variable genes were calculated by Seurat using the variance stabilizing transformation selection
753 method and data were scaled. The variable genes were used to perform principal component analysis
754 (PCA) and the top 20 principal components were used for the unsupervised clustering. Seurat applies
755 a graph-based clustering approach: the "FindNeighbors" function uses the number of principal
756 components (dims = 20) to construct the k-nearest neighbors graph based on the Euclidean distance
757 in PCA space, and the "FindClusters" function applies the Louvain algorithm to iteratively group nuclei
758 (resolution = 1). We then used the PCA embedding to generate an UMAP for cluster visualization. For
759 each cluster, differentially expressed genes (DEGs) were calculated using the "FindMarkers" and
760 "FindAllMarkers" function with default parameters with adjusted $P < 0.05$ using Bonferroni correction.
761 The DEGs were used to assign cell type identity to clusters based on known cell lineage markers
762 described in previously published study[25]. To understand the impact of Paraquat treatment on each
763 cluster, "FindMarkers" function was used to compare "control" vs "Paraquat" treated cells per cluster.
764 Based on the DEGs obtained from this analysis, volcano plots were created using the EnhancedVolcano
765 package v1[47]. UMAP visualizations, feature plots and dot plots for snRNA-seq data were generated
766 using in-built plotting functionality of Seurat.

767 *Subclustering of hemocytes and further analysis:*

768 Based on the cell identity and known hemocyte marker genes from a previous study[25], sub-clusterings
769 were performed using the same unsupervised algorithm and downstream analysis. After removing
770 non-hemocyte clusters, final sub-clustering was done with a modification that "FindNeighbors"
771 function was run with dims = 10 and "FindClusters" function was run with resolution 0.8. Based on the
772 DEGs found by the "FindAllMarkers" function (parameters: only.pos = T, test.use= "MAST") a heat map
773 was plotted for TOP 20 DE genes per clusters.

774 *Subclustering of fat body cells and further analysis:*

775 Based on the cell identity according to the FlyCell Atlas, sub-clustering was performed using the same
776 unsupervised algorithm and downstream analysis as used for hemocytes. After removing non-fat body
777 clusters, final sub-clustering was done with the "FindNeighbors" function which was run with dims =
778 10 and "FindClusters" function which was run with resolution 0.8. Based on the DEGs found by the
779 "FindAllMarkers" function (parameters: only.pos = T, test.use= "MAST") a heat map was plotted for
780 TOP 20 DE genes per clusters.

781 *Regulation network analysis of hemocyte clusters:*

782 In order to determine the transcription factor activity, regulon analysis was performed using the R
783 package SCENIC (v1.3.1)[48]. To remove noise, genes with low expression levels or low positive rates
784 were filtered using the "geneFiltering" function with default settings to obtain a filtered matrix which
785 was used to build co-expression network using the "runCorrelation" and "runGENIE3" functions. Gene
786 regulatory networks (GRNs) were built and scored using the default parameters. Potential regulons
787 based on DNA-motif analysis were selected by using RcisTarget and active gene networks were
788 identified by AUCell. Regulon activity for each cell was calculated as the average normalized expression
789 of putative target genes. Regulon activity matrix was exported which was used to create a new 'AUC'
790 assay using "CreateAssayObject" function of Seurat. "DoHeatmap" function from Seurat was used to
791 plot scaled TF activity in individual hemocytes.

792 *S2 Cell Culture, CellROX staining and flow cytometry:*

793 Drosophila S2 cells (Invitrogen™) were cultured in Schneider's Drosophila medium (Gibco™) at 26°C
794 and atmospheric oxygen and carbon dioxide conditions. The medium contained 10% FCS and 1%
795 penicillin/streptomycin. PQ was added into the medium in concentrations of 15mM or 30mM to
796 investigate the influence on the production of reactive oxygen species (ROS). Control cells remained
797 untreated. To visualize ROS and oxidative stress, the cells were stained with CellROX™ Deep Red
798 Reagent (Invitrogen) for 30 minutes directly in the medium in a concentration of 1:500 at 26°C. The
799 cells were washed twice with 1xPBS containing 2mM EDTA. In order to stain dead cells DAPI was added
800 to the samples in a concentration of 1:1000. Samples were acquired using a BD LSRFortessa™ (BD
801 Biosciences) and analyzed with FlowJo analysis software.

802 *COMET assays:*

803 Comet assays were performed to analyze the amount of DNA damage in S2 cells treated with PQ. S2
804 cells were treated with 15mM or 30mM PQ for 24h. The cells were brought into a concentration of
805 $1.8x10^5$ cells/ml. Low melting agarose (LMA) was boiled at 90°C and subsequently cooled down to 37°C.
806 The cells were diluted in low melting agarose (LMA) at a ratio of 1:10 (cells:LMA) and transferred onto
807 a CometSlide™ (Trevigen). To ensure proper attachment of the LMA, the slides were cooled for 30
808 minutes at 4°C. The lysis was performed for one hour at 4°C. Therefore, the slides were submerged in
809 CometAssay® Lysis Solution (Trevigen). Subsequently the cells were submerged in alkaline unwinding
810 solution (200mM NaOH, 1mM EDTA, pH 13) for 1h at 4°C. The electrophoresis was performed under
811 alkaline conditions (pH13) for 30 minutes with a current of 20V (1V/cm). The slides were neutralized
812 with ddH_2O, dehydrated with 37% ethanol and dried properly at 37°C before they were stained with
813 SYBR™Gold (Invitrogen) for 30 minutes. Comets were imaged with an Olympus BX61 fluorescence
814 microscope. Comet data was analyzed via TriTrek CometScore 2.0.0.38 software.

815 *Statistical analysis and data handling:*

816 Statistical significance of real-time qPCR, Paraquat survival, hemocyte quantification, TLC, Glucose
817 assay, CellROX and comet assay data was calculated with an unpaired t-test or one-way ANOVA as
818 indicated in the figure legends. Lifespan/survival assays were analyzed using Log-Rank and Wilcoxon
819 test. Significance digits indicate the following significance levels: *$p<0.05$, **$p<0.01$, ***$p<0.001$,
820 ****$p<0.0001$. Significance tests were performed using GraphPad Prism 9 software. Data handling of
821 snRNAseq data is described above.

822 **Data availability**

snRNA-seq data will be available upon publication on the gene omnibus express (GEO) platform, GEO accession number: GSE24429. Please contact the lead contact for the token. Microscopy, flow cytometry and survival data reported in this paper will be shared by the lead contact upon request. Any additional information required to reanalyze the data reported in this paper is available from the lead contact upon request.

References

1. Pham-Huy, L.A., He, H., and Pham-Huy, C. (2008). Free Radicals, Antioxidants in Disease and Health. Int J Biomed Sci *4*, 89–96.

2. Sinenko, S.A., Shim, J., and Banerjee, U. (2011). Oxidative stress in the haematopoietic niche regulates the cellular immune response in Drosophila. EMBO Rep *13*, 83–89. 10.1038/embor.2011.223.

3. Herb, M., and Schramm, M. (2021). Functions of ROS in Macrophages and Antimicrobial Immunity. Antioxidants (Basel) *10*, 313. 10.3390/antiox10020313.

4. Nathan, C., and Cunningham-Bussel, A. (2013). Beyond oxidative stress: an immunologist's guide to reactive oxygen species. Nat Rev Immunol *13*, 349–361. 10.1038/nri3423.

5. Finkel, T., and Holbrook, N.J. (2000). Oxidants, oxidative stress and the biology of ageing. Nature *408*, 239–247. 10.1038/35041687.

6. Moghadam, Z.M., Henneke, P., and Kolter, J. (2021). From Flies to Men: ROS and the NADPH Oxidase in Phagocytes. Frontiers in Cell and Developmental Biology *9*, 618. 10.3389/fcell.2021.628991.

7. Meister, M., and Lagueux, M. (2003). Drosophila blood cells. Cell Microbiol *5*, 573–580. 10.1046/j.1462-5822.2003.00302.x.

8. Banerjee, U., Girard, J.R., Goins, L.M., and Spratford, C.M. (2019). Drosophila as a Genetic Model for Hematopoiesis. Genetics *211*, 367–417. 10.1534/genetics.118.300223.

9. Gold, K.S., and Brückner, K. (2014). Drosophila as a model for the two myeloid blood cell systems in vertebrates. Exp. Hematol. *42*, 717–727. 10.1016/j.exphem.2014.06.002.

10. Holz, A., Bossinger, B., Strasser, T., Janning, W., and Klapper, R. (2003). The two origins of hemocytes in Drosophila. Development *130*, 4955–4962. 10.1242/dev.00702.

11. Péan, C.B., Schiebler, M., Tan, S.W.S., Sharrock, J.A., Kierdorf, K., Brown, K.P., Maserumule, M.C., Menezes, S., Pilátová, M., Bronda, K., et al. (2017). Regulation of phagocyte triglyceride by a STAT-ATG2 pathway controls mycobacterial infection. Nat Commun *8*, 14642. 10.1038/ncomms14642.

12. Woodcock, K.J., Kierdorf, K., Pouchelon, C.A., Vivancos, V., Dionne, M.S., and Geissmann, F. (2015). Macrophage-derived upd3 cytokine causes impaired glucose homeostasis and reduced lifespan in Drosophila fed a lipid-rich diet. Immunity *42*, 133–144. 10.1016/j.immuni.2014.12.023.

861 13. Kierdorf, K., Hersperger, F., Sharrock, J., Vincent, C.M., Ustaoglu, P., Dou, J., Gyoergy, A., Groß,
862 O., Siekhaus, D.E., and Dionne, M.S. (2020). Muscle function and homeostasis require cytokine
863 inhibition of AKT activity in Drosophila. Elife *9*, e51595. 10.7554/eLife.51595.

864 14. Ayyaz, A., Li, H., and Jasper, H. (2015). Haemocytes control stem cell activity in the Drosophila
865 intestine. Nat. Cell Biol. *17*, 736–748. 10.1038/ncb3174.

866 15. Myers, A.L., Harris, C.M., Choe, K.-M., and Brennan, C.A. (2018). Inflammatory production of
867 reactive oxygen species by Drosophila hemocytes activates cellular immune defenses.
868 Biochemical and Biophysical Research Communications *505*, 726–732.
869 10.1016/j.bbrc.2018.09.126.

870 16. Fogarty, C.E., Diwanji, N., Lindblad, J.L., Tare, M., Amcheslavsky, A., Makhijani, K., Brückner, K.,
871 Fan, Y., and Bergmann, A. (2016). Extracellular Reactive Oxygen Species Drive Apoptosis-Induced
872 Proliferation via Drosophila Macrophages. Current Biology *26*, 575–584.
873 10.1016/j.cub.2015.12.064.

874 17. Chakrabarti, S., Dudzic, J.P., Li, X., Collas, E.J., Boquete, J.-P., and Lemaitre, B. (2016). Remote
875 Control of Intestinal Stem Cell Activity by Haemocytes in Drosophila. PLoS Genet *12*, e1006089.
876 10.1371/journal.pgen.1006089.

877 18. Chakrabarti, S., and Visweswariah, S.S. (2020). Intramacrophage ROS Primes the Innate Immune
878 System via JAK/STAT and Toll Activation. Cell Reports *33*, 108368. 10.1016/j.celrep.2020.108368.

879 19. Wu, S.-C., Liao, C.-W., Pan, R.-L., and Juang, J.-L. (2012). Infection-Induced Intestinal Oxidative
880 Stress Triggers Organ-to-Organ Immunological Communication in Drosophila. Cell Host &
881 Microbe *11*, 410–417. 10.1016/j.chom.2012.03.004.

882 20. Wang, M.C., Bohmann, D., and Jasper, H. (2003). JNK Signaling Confers Tolerance to Oxidative
883 Stress and Extends Lifespan in Drosophila. Developmental Cell *5*, 811–816. 10.1016/S1534-
884 5807(03)00323-X.

885 21. Cox, N., Crozet, L., Holtman, I.R., Loyher, P.-L., Lazarov, T., White, J.B., Mass, E., Stanley, E.R.,
886 Elemento, O., Glass, C.K., et al. (2021). Diet-regulated production of PDGFcc by macrophages
887 controls energy storage. Science *373*. 10.1126/science.abe9383.

888 22. Martelotto, L. (2020). 'Frankenstein' protocol for nuclei isolation from fresh and frozen tissue for
889 snRNAseq.

890 23. Hao, Y., Hao, S., Andersen-Nissen, E., Mauck, W.M., Zheng, S., Butler, A., Lee, M.J., Wilk, A.J.,
891 Darby, C., Zager, M., et al. (2021). Integrated analysis of multimodal single-cell data. Cell *184*,
892 3573-3587.e29. 10.1016/j.cell.2021.04.048.

893 24. Li, H., Janssens, J., De Waegeneer, M., Kolluru, S.S., Davie, K., Gardeux, V., Saelens, W., David,
894 F.P.A., Brbić, M., Spanier, K., et al. (2022). Fly Cell Atlas: A single-nucleus transcriptomic atlas of
895 the adult fruit fly. Science *375*, eabk2432. 10.1126/science.abk2432.

896 25. Cattenoz, P.B., Sakr, R., Pavlidaki, A., Delaporte, C., Riba, A., Molina, N., Hariharan, N.,
897 Mukherjee, T., and Giangrande, A. (2020). Temporal specificity and heterogeneity of Drosophila
898 immune cells. EMBO J *39*, e104486. 10.15252/embj.2020104486.

899 26. Tattikota, S.G., Cho, B., Liu, Y., Hu, Y., Barrera, V., Steinbaugh, M.J., Yoon, S.-H., Comjean, A., Li,
900 F., Dervis, F., et al. (2020). A single-cell survey of Drosophila blood. eLife *9*, e54818.
901 10.7554/eLife.54818.

902 27. Morales, A.J., Carrero, J.A., Hung, P.J., Tubbs, A.T., Andrews, J.M., Edelson, B.T., Calderon, B.,
903 Innes, C.L., Paules, R.S., Payton, J.E., et al. (2017). A type I IFN-dependent DNA damage response
904 regulates the genetic program and inflammasome activation in macrophages. eLife *6*, e24655.
905 10.7554/eLife.24655.

906 28. Jiang, H., Patel, P.H., Kohlmaier, A., Grenley, M.O., McEwen, D.G., and Edgar, B.A. (2009).
907 Cytokine/Jak/Stat Signaling Mediates Regeneration and Homeostasis in the Drosophila Midgut.
908 Cell *137*, 1343–1355. 10.1016/j.cell.2009.05.014.

909 29. Pastor-Pareja, J.C., Wu, M., and Xu, T. (2008). An innate immune response of blood cells to
910 tumors and tissue damage in Drosophila. Dis Model Mech *1*, 144–154; discussion 153.
911 10.1242/dmm.000950.

912 30. Karpac, J., Younger, A., and Jasper, H. (2011). Dynamic coordination of innate immune signaling
913 and Insulin signaling regulates systemic responses to localized DNA damage. Dev Cell *20*, 841–
914 854. 10.1016/j.devcel.2011.05.011.

915 31. Louradour, I., Sharma, A., Morin-Poulard, I., Letourneau, M., Vincent, A., Crozatier, M., and
916 Vanzo, N. (2017). Reactive oxygen species-dependent Toll/NF-κB activation in the Drosophila
917 hematopoietic niche confers resistance to wasp parasitism. eLife *6*, e25496.
918 10.7554/eLife.25496.

919 32. Paraquat administration in Drosophila for use in metabolic studies of oxidative stress (2011).
920 Analytical Biochemistry *419*, 345–347. 10.1016/j.ab.2011.08.023.

921 33. Jiang, H., Grenley, M.O., Bravo, M.-J., Blumhagen, R.Z., and Edgar, B.A. (2011). EGFR/Ras/MAPK
922 signaling mediates adult midgut epithelial homeostasis and regeneration in Drosophila. Cell Stem
923 Cell *8*, 84–95. 10.1016/j.stem.2010.11.026.

924 34. Patel, P.H., Pénalva, C., Kardorff, M., Roca, M., Pavlović, B., Thiel, A., Teleman, A.A., and Edgar,
925 B.A. (2019). Damage sensing by a Nox-Ask1-MKK3-p38 signaling pathway mediates regeneration
926 in the adult Drosophila midgut. Nat Commun *10*, 4365. 10.1038/s41467-019-12336-w.

927 35. Azad, P., Ryu, J., and Haddad, G.G. (2011). Distinct role of Hsp70 in Drosophila hemocytes during
928 severe hypoxia. Free Radic Biol Med *51*, 530–538. 10.1016/j.freeradbiomed.2011.05.005.

929 36. Huang, K., Chen, W., Zhu, F., Li, P.W.-L., Kapahi, P., and Bai, H. (2019). RiboTag translatomic
930 profiling of Drosophila oenocytes under aging and induced oxidative stress. BMC Genomics *20*,
931 50. 10.1186/s12864-018-5404-4.

932 37. Maitra, U., Scaglione, M.N., Chtarbanova, S., and O'Donnell, J.M. (2019). Innate immune
933 responses to paraquat exposure in a Drosophila model of Parkinson's disease. Sci Rep *9*, 12714.
934 10.1038/s41598-019-48977-6.

935 38. Donovan, M.R., and Marr, M.T. (2016). dFOXO Activates Large and Small Heat Shock Protein
936 Genes in Response to Oxidative Stress to Maintain Proteostasis in Drosophila*. Journal of
937 Biological Chemistry *291*, 19042–19050. 10.1074/jbc.M116.723049.

938 39. Khan, C., Muliyil, S., and Rao, B.J. (2019). Genome Damage Sensing Leads to Tissue Homeostasis
939 in Drosophila. Int Rev Cell Mol Biol *345*, 173–224. 10.1016/bs.ircmb.2018.12.001.

940 40. Dunphy, G., Flannery, S.M., Almine, J.F., Connolly, D.J., Paulus, C., Jønsson, K.L., Jakobsen, M.R.,
941 Nevels, M.M., Bowie, A.G., and Unterholzner, L. (2018). Non-canonical Activation of the DNA

942 Sensing Adaptor STING by ATM and IFI16 Mediates NF-κB Signaling after Nuclear DNA Damage.
943 Mol Cell *71*, 745-760.e5. 10.1016/j.molcel.2018.07.034.

944 41. Bednarski, J.J., and Sleckman, B.P. (2019). At the intersection of DNA damage and immune
945 responses. Nat Rev Immunol *19*, 231–242. 10.1038/s41577-019-0135-6.

946 42. Yang, H., Kronhamn, J., Ekström, J., Korkut, G.G., and Hultmark, D. (2015). JAK/STAT signaling in
947 Drosophila muscles controls the cellular immune response against parasitoid infection. EMBO
948 Rep *16*, 1664–1672. 10.15252/embr.201540277.

949 43. Dionne, M.S., Pham, L.N., Shirasu-Hiza, M., and Schneider, D.S. (2006). Akt and FOXO
950 dysregulation contribute to infection-induced wasting in Drosophila. Curr Biol *16*, 1977–1985.
951 10.1016/j.cub.2006.08.052.

952 44. Yang, H., and Hultmark, D. (2016). Tissue communication in a systemic immune response of
953 Drosophila. Fly (Austin) *10*, 115–122. 10.1080/19336934.2016.1182269.

954 45. Young, M.D., and Behjati, S. (2020). SoupX removes ambient RNA contamination from droplet-
955 based single-cell RNA sequencing data. Gigascience *9*, giaa151. 10.1093/gigascience/giaa151.

956 46. McGinnis, C.S., Murrow, L.M., and Gartner, Z.J. (2019). DoubletFinder: Doublet Detection in
957 Single-Cell RNA Sequencing Data Using Artificial Nearest Neighbors. Cell Syst *8*, 329-337.e4.
958 10.1016/j.cels.2019.03.003.

959 47. Blighe, K. (2021). EnhancedVolcano: publication-ready volcano plots with enhanced colouring
960 and labeling.

961 48. Aibar, S., González-Blas, C.B., Moerman, T., Huynh-Thu, V.A., Imrichova, H., Hulselmans, G.,
962 Rambow, F., Marine, J.-C., Geurts, P., Aerts, J., et al. (2017). SCENIC: single-cell regulatory
963 network inference and clustering. Nat Methods *14*, 1083–1086. 10.1038/nmeth.4463.

964 49. Hersperger, F., Kastl, M., Paeschke, K., and Kierdorf, K. (2024). Hemocyte Nuclei Isolation from
965 Adult Drosophila melanogaster for snRNA-seq. Methods Mol Biol *2713*, 71–79. 10.1007/978-1-
966 0716-3437-0_4.

967 **Figure Legends**

968

969 **Figure 1. Loss of hemocytes increases the susceptibility of adult Drosophila to oxidative stress by**
970 **Paraquat feeding.** (A) Survival of *Hml/+* flies with control food (C) (n=20) and 15mM Paraquat (P)
971 (n=28) at 29°C. Five independent experiments were performed. Student's unpaired t-test:
972 ****p<0.0001, each data point represents a sample with 10 flies. (B-C) RT-qPCR of whole flies were
973 performed to investigate gene-expressions of the JAK-STAT-signaling pathway (B) and insulin-signaling
974 pathway (C). All transcript levels were normalized to the expression of the loading control *Rpl1* and are
975 shown in arbitrary units [au]. Each data point (n=5) represents a sample of three whole flies. Student's
976 unpaired t-tests were performed for each transcript to compare the gene-expression between control
977 and treated flies: **p<0.01; ***p<0.001; ****p<0.0001. (D) Glucose and (E) glycogen levels of whole
978 flies were measured in control and PQ-treated flies. Each dot (n=3) represents a sample containing
979 three flies. Student's unpaired t-test: **p<0.01. (F) Triglyceride (TG) amounts were determined via
980 thin-layer chromatography (TLC). Left panel: Representative image of a TLC plate, each band
981 represents a sample with ten flies. Right panel: Quantification thereof. n= 3 per group were analyzed.
982 Student's unpaired t-test: **p<0.01. (G) Representative images of 7 days old *HmlΔ4>eGFP* flies treated

983 with 5% sucrose solution and 15mM PQ respectively. Scale bars = 500µm. (H) Hemocyte quantification
984 of 7 days old *HmlΔ4>eGFP* flies treated with control food (5% sucrose solution) (n=5) or 15mM
985 Paraquat (n=5). Each data point represents one fly. Statistical significance was tested using student's
986 unpaired t-test: p=0.508. (I) Survival of *crq-Gal80^{ts}/+* control flies (n=13) and hemocyte depleted *crq-*
987 *Gal80^{ts}>reaper* flies (n=7) on control food (n=20) and 15mM Paraquat (n=28) at 29°C. Student's
988 unpaired t-test: ****p<0.0001, each data point represents a sample with 10 flies. (J) TG amounts in
989 *crq-Gal80^{ts}/+* control flies and hemocyte-deficient *crq-Gal80^{ts}>reaper* flies on control food or Paraquat
990 food. Left panel: Representative image of a TLC plate, each band represents a sample with ten flies.
991 Right panel: Quantification thereof. n= 3 per group were analyzed. One-way ANOVA: *p<0.05. (K)
992 Glucose and (L) Glycogen levels of whole flies were measured in *crq-Gal80^{ts}/+* control flies and
993 hemocyte-deficient *crq-Gal80^{ts}>reaper* flies. Each dot (n= 3) represents a sample with three whole
994 flies. One-way ANOVA: ****p<0.0001.

995 **Figure 2. Unbiased single nuclei transcriptomic profiling identified diverse transcriptomic states of**
996 **hemocytes associated with oxidative stress response.** (A) Uniform Manifold Approximation and
997 Projection (UMAP) visualization of single nucleus states from flies exposed to 15mM PQ containing or
998 control food. Dashed lines indicate the broad cell types. Male accessory gland main cells (MAG),
999 Malpighian tubule principal cells (MTC), male germline cells (MGC), outer photoreceptor cells (PRC),
1000 tracheolar cells (TC), epithelial cells (EC). Colors indicate distinct clusters. n=11839 nuclei are shown.
1001 (B) UMAP visualization of nuclei from **A** colored by treatment. Nuclei from control group are labeled
1002 in red and nuclei from PQ group are labeled in blue. Dashed lines indicate the broad cell type as **A**. (C)
1003 UMAP visualization of hemocytes from **A** after sub-setting and re-clustering. Colors and dashed lines
1004 indicate distinct clusters. n=1354 nuclei are shown. (D) UMAP visualization of hemocyte clusters
1005 colored by treatment. Nuclei from control group are labeled in red and nuclei from PQ group are
1006 labeled in blue. Dashed lines indicate distinct clusters. n=1354 nuclei are shown. (E) Heat map of top
1007 20 DE genes for each hemocyte cluster. Gene names are indicated on the left. Colors in the heat map
1008 correspond to normalized scaled expression. (F) Volcano plots comparing pseudo bulk gene expression
1009 of individual hemocyte cluster vs. all hemocytes. The $-\log_{10}$-transformed adjusted P value (P adjusted,
1010 y-axis) is plotted against the $\log_2$-transformed fold change (FC) in expression between the indicated
1011 cluster vs remaining hemocytes (x-axis). Non-regulated genes are shown in grey, not significantly
1012 regulated genes are shown in green, significantly regulated genes with a FC<1.5 are shown in blue and
1013 significantly regulated genes with a FC>1.5 are shown in red.

1014 **Figure 3: A specific cluster of plasmatocytes responds to oxidative stress with immune activation by**
1015 **Jak/STAT, DDR and JNK signaling.** (A) Key transcription factors (TFs) regulating hemocytes states. Heat
1016 map of scaled TF activity at a single cell level in hemocytes states from **Figure 2C**. Colors in the heat
1017 map correspond to scaled expression. Numbers on top indicate the cluster identity. Labels on the left
1018 and right indicate the TFs. (B) Feature plots showing scaled expression of selected genes associated
1019 with JAK/STAT signaling (*upd3*, *Socs36E*, *TotA*, *TotM*, *Fas3*), JNK and DNA damage signaling (*puc*,
1020 *Gadd45*), insulin signaling (*Thor*, *InR*), TGFβ signaling (*dpp*, *daw*) and TNF signaling (*egr*).

1021 **Figure 4**: **Oxidative stress induced different transcriptomic states in fat body cells, including cells with**
1022 **a distinct Jak/STAT activation signature** (A) UMAP visualization of fat body cells from **Figure 2A** by
1023 unsupervised clustering. Colors and dashed lines indicate different clusters. Each dot represents one
1024 nucleus. n=3150 nuclei are shown. (B) UMAP of fat body cell clusters split by treatment. Nuclei from
1025 control flies are labeled in red and nuclei from PQ treated flies are labeled in blue. Dashed lines indicate
1026 different clusters. Each dot represents one nucleus. n=3150 nuclei are shown. (C) Heat map of top 20

1027 DE genes for each fat body cluster. Gene names indicated on the left. Fold change of gene expression
1028 is color coded as indicated in legend. (F) Volcano plots comparing pseudo bulk gene expression of
1029 individual fat body cluster vs. all fat body cells. The $-\log_{10}$-transformed adjusted P value (P adjusted, y-
1030 axis) is plotted against the $\log_2$-transformed fold change (FC) in expression between the indicated
1031 cluster vs remaining hemocytes (x-axis). Non-regulated genes are shown in grey, not significantly
1032 regulated genes are shown in green, significantly regulated genes with a FC<1.5 are shown in blue and
1033 significantly regulated genes with a FC>1.5 are shown in red.

1034 **Figure 5: Loss of DNA damage signaling activity in hemocytes leads to an increase in systemic *upd3***
1035 **levels and a higher susceptibility to oxidative stress**. (A) Survival of *Hml/+* (n= 28), *Hml>mei41-IR (n*=
1036 23); *Hml>tefu-IR (n*= 24); *Hml>mei41-IR,tefu-IR (n*= 16) and *Hml>nbs-IR* (n= 22) flies on control food
1037 and PQ. Each data point represents a sample of 10 flies. Mean ± SEM is shown. Three independent
1038 experiments were performed. One-way ANOVA: ****p<0.001*; *****p<0.0001*. (B) Hemocyte
1039 quantification of *Hml/+* control flies and DDR-knockdowns on control food (C) and 15mM Paraquat (P).
1040 Each data point represents one fly (n=5 for all groups). Mean ± SEM is shown. One way ANOVA: *Hml/+*
1041 (C) vs *Hml>tefu-IR* (C), ***p=0.0052*; *Hml>tefu-IR* (C) vs *Hml>tefu-IR* (P), **p=0.03* (C) Comet assay of
1042 isolated hemocytes from *Hml/+* (C: n=73; P: n=129), *Hml>mei41-IR* (C: n=119; P: n=132) and *Hml>tefu-*
1043 *IR* (C: n=175; P: n=125) - flies on control food and PQ. Olive tail moment of comet assays of sorted
1044 hemocyte nuclei is shown. One-way ANOVA: *p<0.05; ***p<0.001; ****p<0.0001. (D) Gene
1045 expression analysis for *Jak/STAT* target genes via RT-qPCR in *Hml/+* control flies and DDR-knockdowns
1046 on control food (C) and 15mM Paraquat (P). All transcript levels were normalized to the expression of
1047 the loading control *Rpl1* and are shown in arbitrary units [au]. Each data point (n=5) represents a
1048 sample of three individual flies. Mean ± SEM is shown. Two-way ANOVA: **p<0.05*; ***p<0.01*; ***
1049 *p<0.001*; *****p<0.0001*. (E) Gene expression analysis for insulin signaling target genes and *Ilps* via RT-
1050 qPCR in *Hml/+* control flies and DDR-knockdowns on control food (C) and 15mM Paraquat (P). All
1051 transcript levels were normalized to the expression of the loading control *Rpl1* and are shown in
1052 arbitrary units [au]. Each data point (n=5) represents a sample of three individual flies. Mean ± SEM is
1053 shown. Two-way ANOVA: **p<0.05*; ***p<0.01*; *** *p<0.001*; *****p<0.0001*. (F) Triglyceride (TG) levels
1054 of *Hml/+*, *Hml>mei41-IR*, *Hml>tefu-IR, Hml>mei41-IR,tefu-IR* and *Hml>nbs-IR* flies on control food and
1055 PQ determined via thin-layer chromatography (TLC). One representative TLC is shown (left panel).
1056 Quantification thereof is shown on the right. Each data point (n=4 per group) represents a sample of
1057 ten individual flies. Mean ± SEM is shown. n.d. = not detectable. One-way ANOVA was performed for
1058 both groups (15mM PQ and control) separately: **p=0.0106*.

1059 **Figure 6: Hemocyte-derived *upd3* controls susceptibility to oxidative stress in adult *Drosophila***. (A)
1060 Survival of *Hml/+* (n=28), *Hml>upd3-IR* (n=27) and *Hml>upd3* (n=26) flies on 15mM PQ food. Each data
1061 point represents a sample of 10-15 flies. Mean ± SEM is shown. Three independent experiments were
1062 performed. One-way ANOVA: *****p<0.0001*. (B) Gene expression analysis for *upd3* via RT-qPCR in
1063 *Hml/+, Hml>upd3-IR* and *Hml>upd3* flies on control food (C) and 15mM Paraquat (P). Each data point
1064 (n=5-6) represents a sample of three individual flies. Mean ± SEM is shown. Two-way ANOVA:
1065 *****p<0.0001*. (C) Hemocyte quantifications in *Hml/+, Hml>upd3-IR* and *Hml>upd3* flies on control
1066 food and 15mM PQ food. Each data point represents one fly (n= 5-6). Mean ± SEM is shown. One-way
1067 ANOVA: **p<0.01. (D) Survival of *Hml/+* (n=241), *upd3^{null};Hml/+* (n=122), *Hml>upd3* (n=104),
1068 *upd3^{null};Hml>upd3* (n=57), *Hml>mei-41-IR;tefu-IR* (n=103) and *upd3^{null};Hml>mei-41-IR;tefu-IR* (n=50)
1069 flies on 15mM PQ food at 29°C. Each data point represents a sample with 10-15 flies. Mean ± SEM is
1070 shown. One-way ANOVA: *****p<0.0001*. (E) Survival of *Hml/+* (n=78), *Hml>hep[act]* (n=38) and
1071 *Hml>bsk-DN* (n=80) flies on 15mM PQ food. Each data point represents a sample with 10 flies. Mean ±

1072 SEM is shown. One-way ANOVA: ***p<0.01*; ****p<0.0001*. (F) Gene expression analysis for *upd3* via
1073 RT-qPCR of *Hml/+*, *Hml>hep[act]* and *Hml>bsk-DN* flies on control food (-) and 15mM Paraquat (+).
1074 Each data point (n=5-6) represents a sample of three individual flies. Mean ± SEM is shown. Two-way
1075 ANOVA: **p<0.05.*

1076 **Supplementary Figure Legends**

1077

1078 **Figure S1: Paraquat-induced oxidative stress does not cause gut leakage, but detrimental changes in**
1079 **triglyceride storage in the fat body.** (A) Survival of *Hml/+* flies treated with control food (n=8), 2mM
1080 PQ (n=8), 15mM PQ (n=9) and 30mM PQ (n=8). Each data point represents a sample of 10 flies. Mean
1081 ± SEM is shown. One-way ANOVA: ***p<0.01*; ****p<0.0001*. (B) Smurf assay to test the gut integrity
1082 of 7 days old *Hml/+* flies treated with 2mM PQ (n=79), 15mM PQ (n=90), 30mM PQ (n=80) and controls
1083 (n=80). Data was pooled from two independent experiments. (C) Gene expression analysis for *AMP*
1084 genes via RT-qPCR in whole flies on control food (C) and 15mM Paraquat (P). All transcript levels were
1085 normalized to the expression of the loading control *Rpl1* and are shown in arbitrary units [au]. Each
1086 data point (n=5) represents a sample of three individual flies. Mean ± SEM is shown. (D) Gene
1087 expression analysis for *dpp*, *daw* and *eiger* via RT-qPCR in whole flies on control food (C) and 15mM
1088 Paraquat (P). All transcript levels were normalized to the expression of the loading control *Rpl1* and
1089 are shown in arbitrary units [au]. Each data point (n=5) represents a sample of three individual flies.
1090 Mean ± SEM is shown. (E) Representative light microscopic images of HE stained control flies (left
1091 panels) and flies treated with 15mM PQ (right panels). Inserts indicate location of higher magnification
1092 images below. Scale bar (overview) = 500 µm, scale bar (inserts) = 100 µm. (F) Representative light
1093 microscopic images of Oil Red O stained control flies (left panels) and flies treated with 15mM PQ (right
1094 panels). Arrows indicate stained fat droplets. Scale bar = 100 µm.

1095 **Figure S2: Gating strategy for the FACS isolation of nuclei from control and PQ-treated flies.** (A) Flow
1096 cytometric sorting strategy of nuclei used for the snRNA-seq. Doublet exclusion was performed via
1097 gating on DRAQ7 single positive nuclei. $DRAQ7^{+}DAPI^{+}$ double positive events were considered to be
1098 nuclei and were sorted for the snRNA-seq as previously described[49]. (B) Violin plot indicating number
1099 of genes identified in analyzed nuclei of the sorted samples. Color code is indicated in legend. (C) Violin
1100 plot indicating RNA counts of the analyzed nuclei of each sorted sample. Color code is indicated in
1101 legend. (D) Violin plot indicating percentage of mitochondrial genes detected in the nuclei of each
1102 sorted samples. Color code is indicated in legend.

1103 **Figure S3: Specific signature genes identify plasmatocyte and crystal cell clusters within the eight**
1104 **identified hemocyte clusters.** (A) Dot plot of hemocyte signature gene expression according to
1105 Cattenoz et al[25]. Color code is indicated in legend. (B)-(L) Feature plots for expression levels of
1106 respective hemocyte signature genes across all hemocyte clusters. Color-code, indicating the
1107 expression levels of the respective genes, is shown on the right side of each graph. Gene names are
1108 indicated above plots shown. (M) Bar plot representing distribution of nuclei derived from flies under
1109 control condition (red) and flies treated with 15mM PQ (turquoise) across all eight identified hemocyte
1110 clusters. Each cluster is shown as one bar. Total number of hemocytes in the respective cluster is
1111 indicated below.

1112 **Figure S4: Fat body signature genes are highly expressed across the eight distinct fat body cell**
1113 **clusters and are absent in hemocyte cell clusters.** (A) Dot plot of fat body signature gene expression
1114 according to the Fly Cell Atlas signature[24] on the eight identified hemocytes clusters. Color code is
1115 indicated in legend. (B) Dot plot of fat body signature gene expression on the eight identified fat body
1116 clusters. Color code is indicated in the legend. (C) Dot plot of hemocyte signature gene expression
1117 according to Cattenoz et al.[25] on the eight identified fat body clusters. Color code is indicated in the
1118 legend. (D) Bar plot representing distribution of nuclei derived from flies under control condition (red)

1119 and flies treated with 15mM PQ (turquoise) across all eight identified fat body clusters. Each cluster is
1120 shown as one bar. Total number of fat body cells in the respective cluster is indicated below.

1121 **Figure S5: PQ treatment of S2 cells *in vitro* induces reactive oxygen species, immune activation and**
1122 **DNA damage.** (A) Gating strategy of flow cytometric analysis of control or PQ-treated S2-cells stained
1123 for reactive oxygen species (ROS) with CellROX. Control cells, 15mM PQ treated and 30mM PQ treated
1124 cells are shown in the first, second and third row respectively. After doublet exclusion, dead cells were
1125 excluded via DAPI staining. The amount of ROS was determined in the last gate were the CellROX
1126 staining is shown. (B) Representative FACS histograms of cells treated with PQ and analyzed via CellROX
1127 staining. Gates indicate the cut-off for determining CellROX$^+$ cells. (C) Mean fluorescence intensity
1128 (MFI) of FACS analyzed, CellROX$^+$ cells. Data were generated from three independent experiments
1129 (n=3). One-way ANOVA: **p<0.05; **p<0.01; ***p<0.001; ****p<0.0001*. (D) Comet assay of S2 cells
1130 treated without PQ (n=351), 5mM PQ (n=208), 10mM PQ (n=129) and 15mM PQ (n=71). Assay was
1131 performed in two independent experiments. Data of one representative assay are shown as violin plots
1132 with median (red), second and third quartile. One-way ANOVA: ****p<0.001; ****p>0.0001*. (E-F) Gene
1133 expression analysis of genes associated with JAK-STAT signaling, JNK signaling, insulin signaling is
1134 shown in (E) and TGFβ signaling and AMPs is shown in (F). S2-cells treated with 15mM PQ for six or 24
1135 hours. Controls were untreated. Each dot represents a sample containing RNA of 50.000 cells. One-
1136 way ANOVA: **p<0.05; **p<0.01; ***p<0.001; ****p<0.0001*.

1137 **Figure S6: Loss of DNA damage, upd3 or JNK signaling in hemocytes alters susceptibility to oxidative**
1138 **stress but not overall lifespan.** (A) Representative images of *Hml/+* flies and DDR-Knockdown flies on
1139 control food (left panels) and treated with 15mM PQ (right panels). Five individual flies per group were
1140 analyzed. (B) Lifespan analysis of *Hml/+* (n=251), *Hml>mei-41-IR* (n=231), *Hml>tefu-IR* (n=219),
1141 *Hml>mei-41-IR;tefu-IR* (n=144) and *Hml>nbs-IR* flies (n=299). *Hml/+* vs. *Hml>mei-41-IR*: Log-rank test
1142 *****p<0.0001*, X^2=172.2; Wilcoxon test *****p<0.0001*, X^2=155.9. *Hml/+* vs. *Hml>tefu-IR*: Log-rank test
1143 *****p<0.0001*, X^2=56.09; Wilcoxon test *****p<0.0001*, X^2=50.95. *Hml/+* vs. *Hml>mei-41-IR;tefu-IR*:
1144 Log-rank test ns, X^2=3.1; Wilcoxon test ****p=0.0005*, X^2=12.11. *Hml/+* vs *Hml>nbs-IR*: Log-rank test
1145 *****p<0.0001*, X^2=60.90; Wilcoxon test *****p<0.0001*, X^2=50.21. Data was obtained from three
1146 independent experiments. (C) Starvation survival of *Hml/+* (n=607), *Hml>mei-41-IR* (n=421), *Hml>tefu-*
1147 *IR* (n=480), *Hml>mei-41-IR;tefu-IR* (n=266) and *Hml>nbs-IR* (n=341) flies. *Hml/+* vs. *Hml>mei-41-IR*: Log-
1148 rank test ***p=0.0052*, X^2=7.81; Wilcoxon test ns, X^2=0.02. *Hml/+* vs. *Hml>tefu-IR*: Log-rank test ns,
1149 X^2=0.03; Wilcoxon test **p=0.0153*, X^2=5.88. *Hml/+* vs. *Hml>mei-41-IR;tefu-IR*: Log-rank test ns, X^2=0.21;
1150 Wilcoxon test **p=0.019*, X^2=5.51. *Hml/+* vs *Hml>nbs-IR*: Log-rank test ****p=0.0003*, X^2=13.30; Wilcoxon
1151 test ns, X^2=1.24. Data was obtained from two independent experiments. (D) Lifespan analysis of *Hml-*
1152 *Gal80^{ts}/+* (n=127), *Hml-Gal80^{ts}>mei-41-IR* (n=140), *Hml-Gal80^{ts}>tefu-IR* (n=164), *Hml-Gal80^{ts}>mei-41-*
1153 *IR;tefu-IR* (n=101) and *Hml-Gal80^{ts}>nbs-IR* flies (n=157). *Hml-Gal80^{ts}/+* vs. *Hml-Gal80^{ts}>mei-41-IR*: Log-
1154 rank test *****p<0.0001*, chi^2=21.80; Wilcoxon test *****p<0.0001*, X^2=18.48. *Hml-Gal80^{ts}/+* vs. *Hml-*
1155 *Gal80^{ts}>tefu-IR*: Log-rank test ****p=0.0003*, X^2=13.20; Wilcoxon test **p=0.033*, X^2=4.56. *Hml-Gal80^{ts}/+*
1156 vs. *Hml-Gal80^{ts}>mei-41-IR;tefu-IR*: Log-rank test **p=0.0429*, X^2=4.10; Wilcoxon test ****p=0.0001*,
1157 X^2=14.95. *Hml-Gal80^{ts}/+* vs *Hml-Gal80^{ts}>nbs-IR*: Log-rank test ***p=0.0047*, X^2=7.99; Wilcoxon test ns,
1158 X^2=1.68. Data was obtained from five independent experiments. (E) Survival of *Hml-Gal80^{ts}/+* (n=23),
1159 *Hml-Gal80^{ts}>mei-41-IR* (n=28), *Hml-Gal80^{ts}>tefu-IR* (n=18), *Hml-Gal80^{ts}>mei-41-IR;tefu-IR* (n=13) and
1160 *Hml-Gal80^{ts}>nbs-IR* flies (n=31) on PQ food. Each dot represents a sample with ten flies. Mean ± SEM
1161 is shown. One-way ANOVA **p<0.05*; *****p<0.0001*. Data was obtained from five independent
1162 experiments. (F) Representative images of *Hml/+, Hml>upd3-IR* and *Hml>upd3* flies on control food
1163 (left panels) and treated with 15mM PQ (right panels). Six individual flies per group were analyzed. (G)

1164 Lifespan analysis of *Hml/+ (n=266), Hml>upd3-IR (n=269),* and *Hml>upd3* flies (n=193). *Hml/+* vs.
1165 *Hml>upd3-IR*: Log-rank test ****$p<0.0001$, X^2=96.03; Wilcoxon test ****$p<0.0001$, X^2=81.16. *Hml/+*
1166 vs. *Hml>upd3*: Log-rank test ****$p<0.0001$, X^2=15.33; Wilcoxon test *$p=0.0124$, X^2=6.26. Results are
1167 shown from two independent experiments. (H) Lifespan analysis of *Hml/+* (n=281), *Hml>hep[act]*
1168 (n=117), and *Hml>bsk-DN* (n=273) flies. *Hml/+* vs. *Hml>hep[act]*; Log-rank test: n.s.; p=0.69, X^2=0.16;
1169 Wilcoxon test: n.s. p=0.18, X^2=1.77. *Hml/+* vs. *Hml>bsk-DN*: Log-rank test: ****$p<0.0001$, X^2=25.31;
1170 Wilcoxon test: ****$p<0.0001$, X^2=23.61. Data was obtained from two independent experiments.

1171 **Table S1: Differentially expressed genes in hemocyte clusters C1-C8.**

1172 **Table S2: Differentially expressed genes in fat body cell clusters C1-C8.**

1173 **Table S3: Transgenic *Drosophila* lines and primers used in the study.**

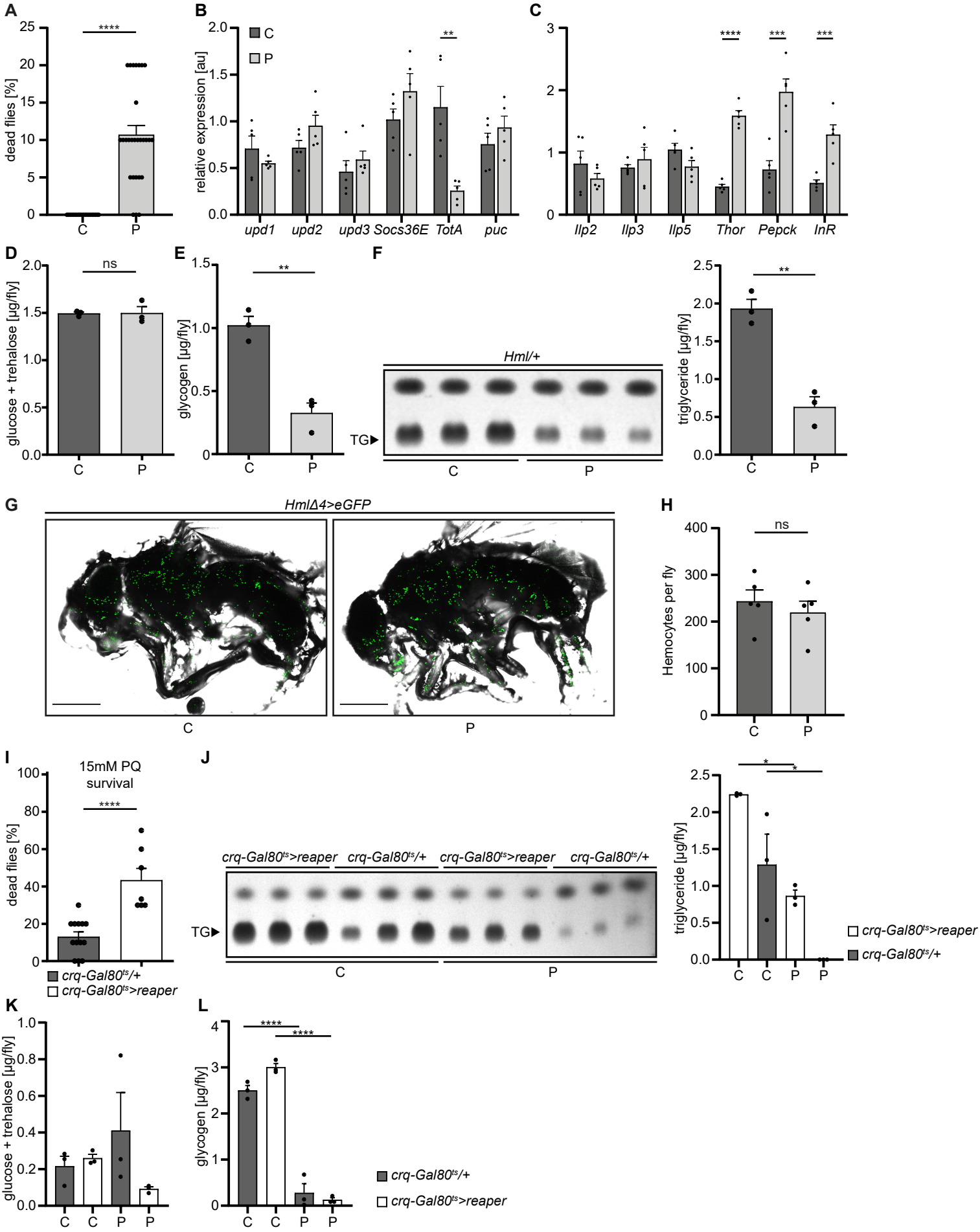
A
dead flies [%]
****
C
P
B
relative expression [au]
C
P
**
upd1
upd2
upd3
Socs36E
TotA
puc
C
Ilp2
Ilp3
Ilp5
Thor
Pepck
InR
****
***
***
D
glucose + trehalose [µg/fly]
ns
E
glycogen [µg/fly]
**
F
Hml/+
TG
triglyceride [µg/fly]
**
G
HmlΔ4>eGFP
H
Hemocytes per fly
ns
I
15mM PQ
survival
dead flies [%]
****
crq-Gal80ts/+
crq-Gal80ts>reaper
J
crq-Gal80ts>reaper
crq-Gal80ts/+
crq-Gal80ts>reaper
crq-Gal80ts/+
TG
triglyceride [µg/fly]
*
*
crq-Gal80ts>reaper
crq-Gal80ts/+
K
glucose + trehalose [µg/fly]
L
glycogen [µg/fly]
****
****
crq-Gal80ts/+
crq-Gal80ts>reaper

Figure 1

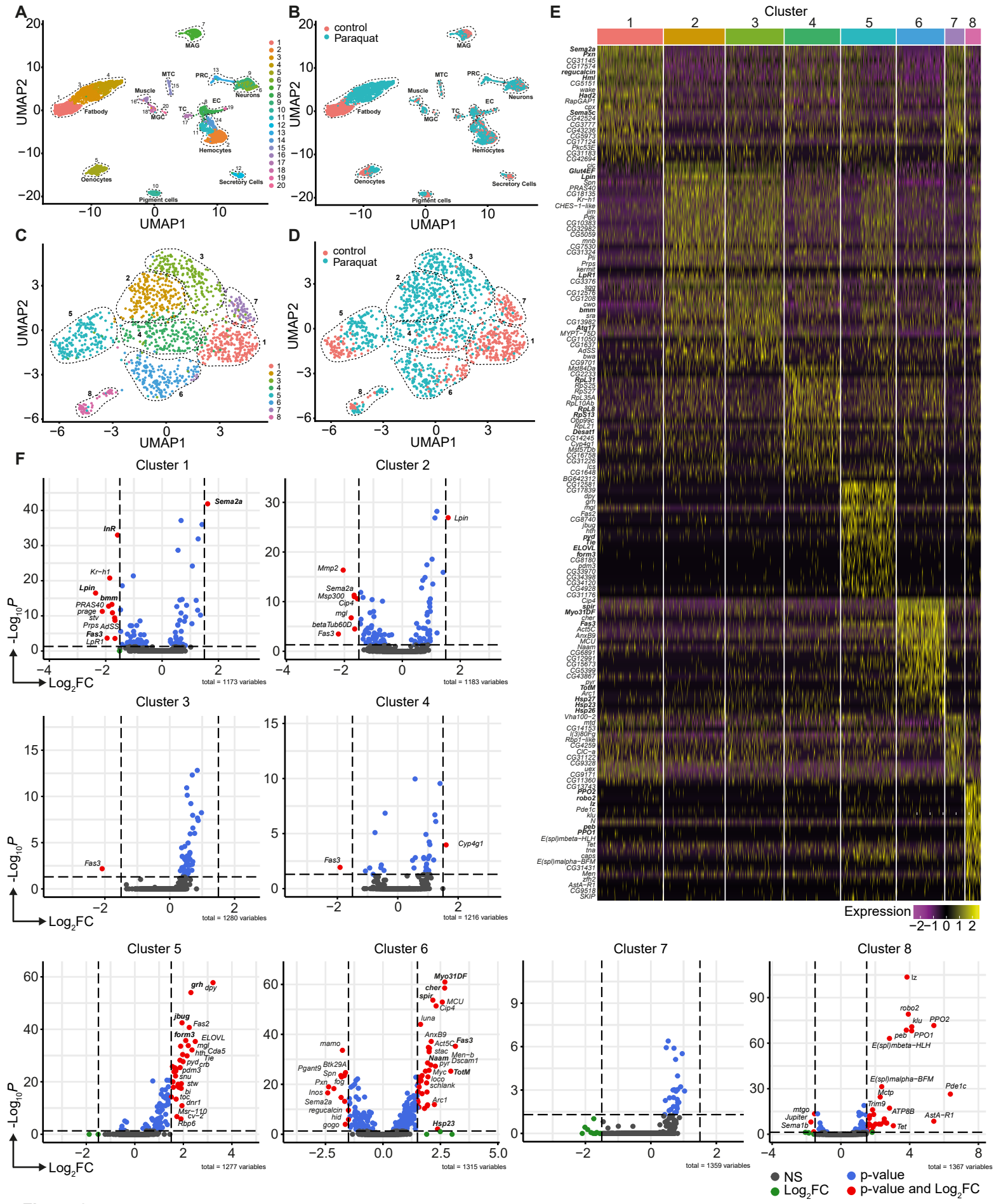
A
B
C
D
E
F
UMAP1
UMAP2
control
Paraquat
MAG
MTC
PRC
Muscle
Neurons
Fatbody
MGC
TC
EC
Hemocytes
Oenocytes
Secretory Cells
Pigment cells
Cluster
Expression
Cluster 1
Cluster 2
Cluster 3
Cluster 4
Cluster 5
Cluster 6
Cluster 7
Cluster 8
-Log10P
Log2FC
total = 1173 variables
total = 1183 variables
total = 1280 variables
total = 1216 variables
total = 1277 variables
total = 1315 variables
total = 1359 variables
total = 1367 variables
NS
Log2FC
p-value
p-value and Log2FC

Figure 2

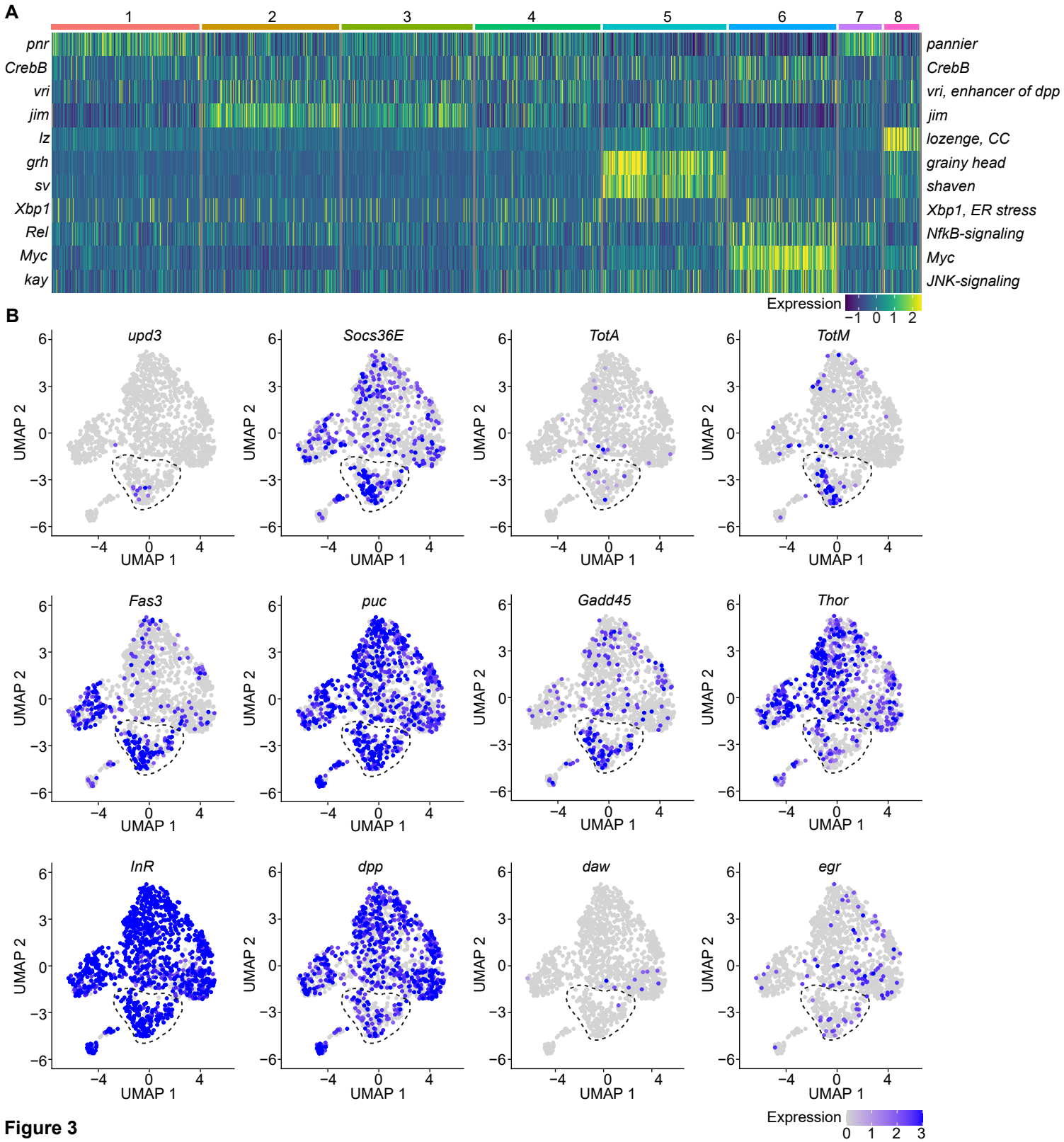
A
1
2
3
4
5
6
7
8
pnr
CrebB
vri
jim
lz
grh
sv
Xbp1
Rel
Myc
kay
pannier
CrebB
vri, enhancer of dpp
jim
lozenge, CC
grainy head
shaven
Xbp1, ER stress
NfkB-signaling
Myc
JNK-signaling
Expression
−1 0 1 2
B
upd3
Socs36E
TotA
TotM
Fas3
puc
Gadd45
Thor
InR
dpp
daw
egr
UMAP 1
UMAP 2
Expression
0 1 2 3

Figure 3

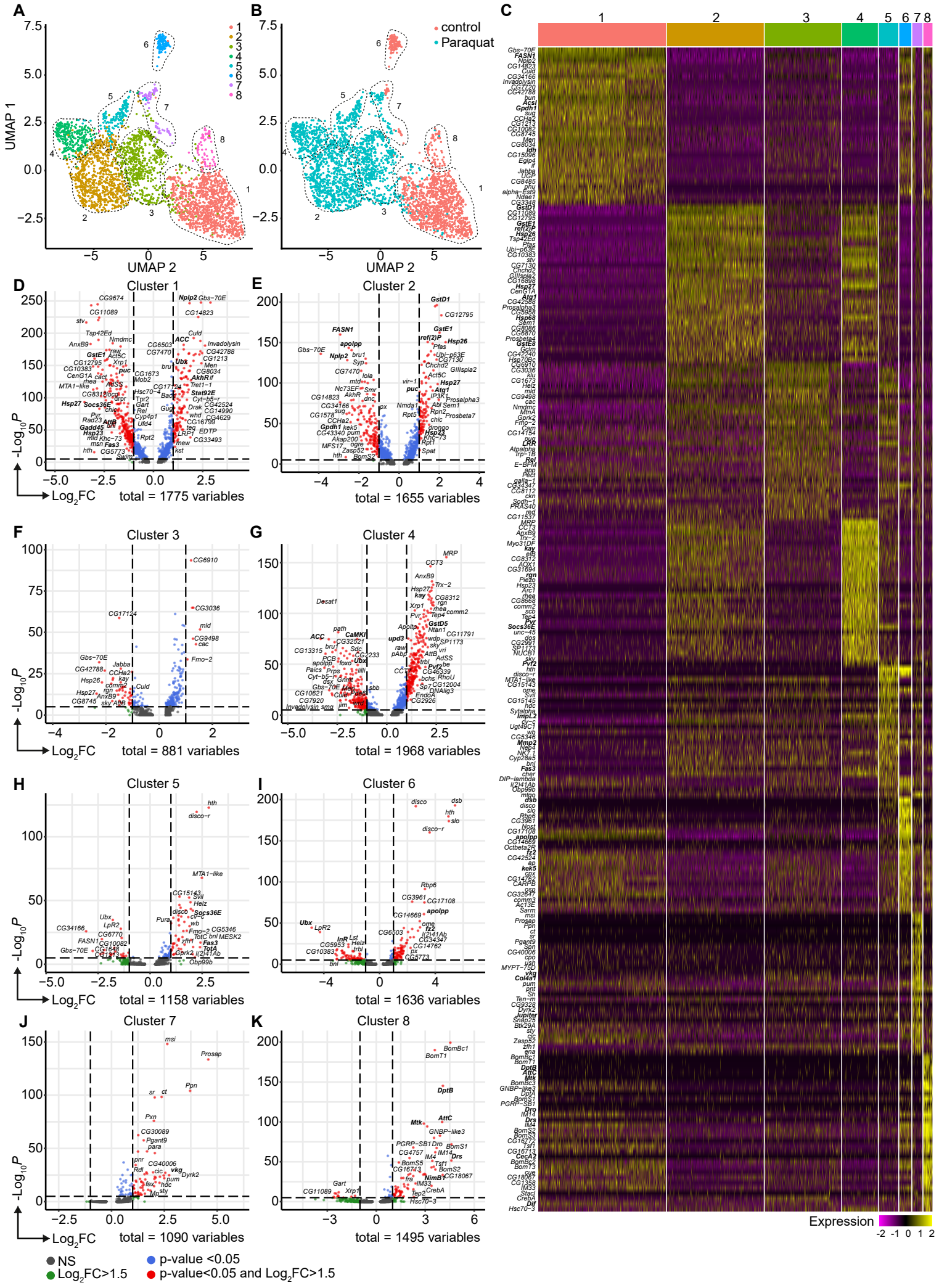
A
B
C
UMAP 1
UMAP 2
control
Paraquat
Expression
D
Cluster 1
total = 1775 variables
E
Cluster 2
total = 1655 variables
F
Cluster 3
total = 881 variables
G
Cluster 4
total = 1968 variables
H
Cluster 5
total = 1158 variables
I
Cluster 6
total = 1636 variables
J
Cluster 7
total = 1090 variables
K
Cluster 8
total = 1495 variables
-Log10P
Log2FC
NS
Log2FC>1.5
p-value <0.05
p-value<0.05 and Log2FC>1.5

Figure 4

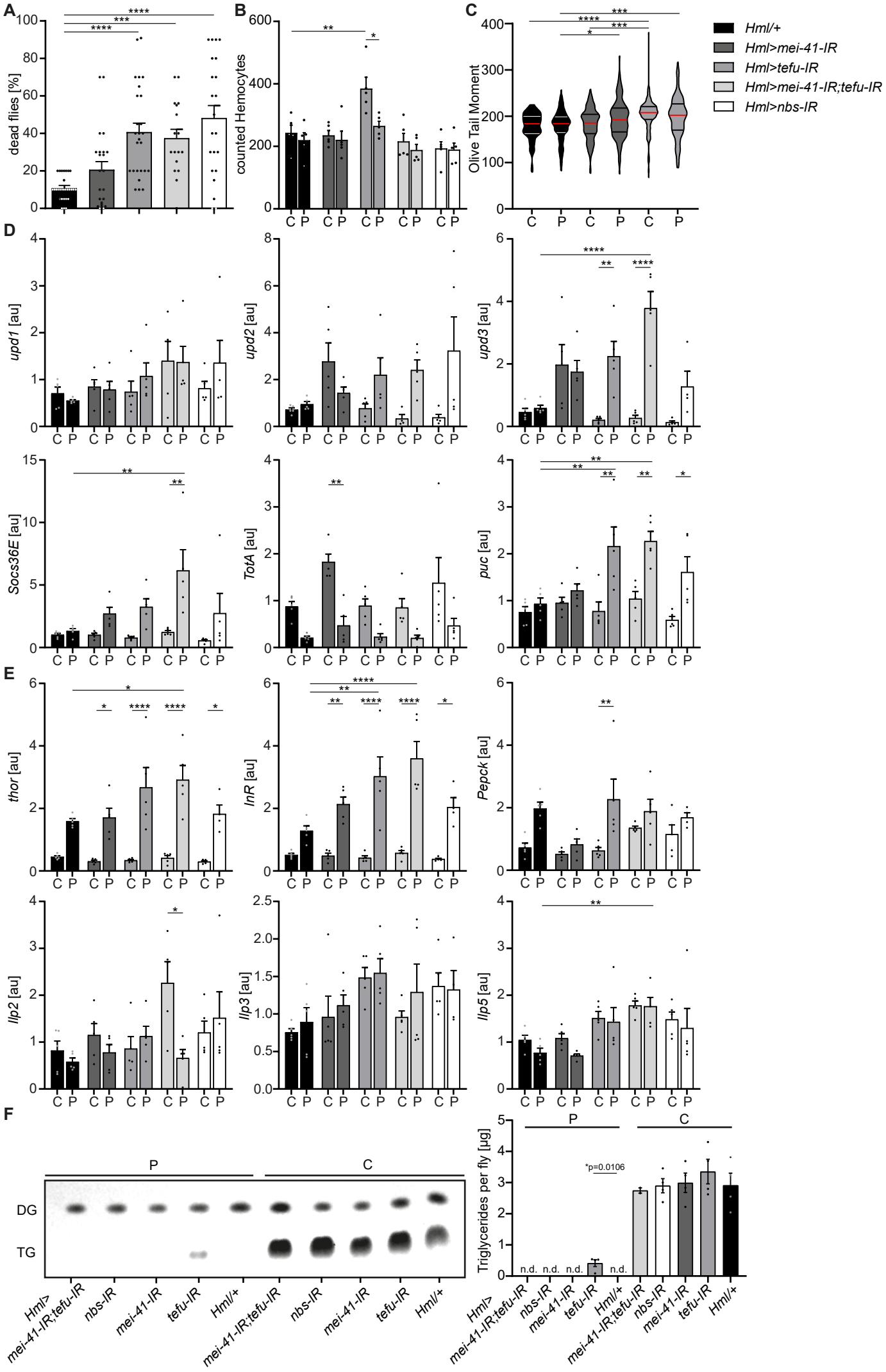
A
dead flies [%]
B
counted Hemocytes
C
Olive Tail Moment
Hml/+
Hml>mei-41-IR
Hml>tefu-IR
Hml>mei-41-IR;tefu-IR
Hml>nbs-IR
D
upd1 [au]
upd2 [au]
upd3 [au]
Socs36E [au]
TotA [au]
puc [au]
E
thor [au]
InR [au]
Pepck [au]
Ilp2 [au]
Ilp3 [au]
Ilp5 [au]
F
P
C
DG
TG
Triglycerides per fly [µg]
*p=0.0106
n.d.
Hml>mei-41-IR;tefu-IR
nbs-IR
mei-41-IR
tefu-IR
Hml/+

Figure 5

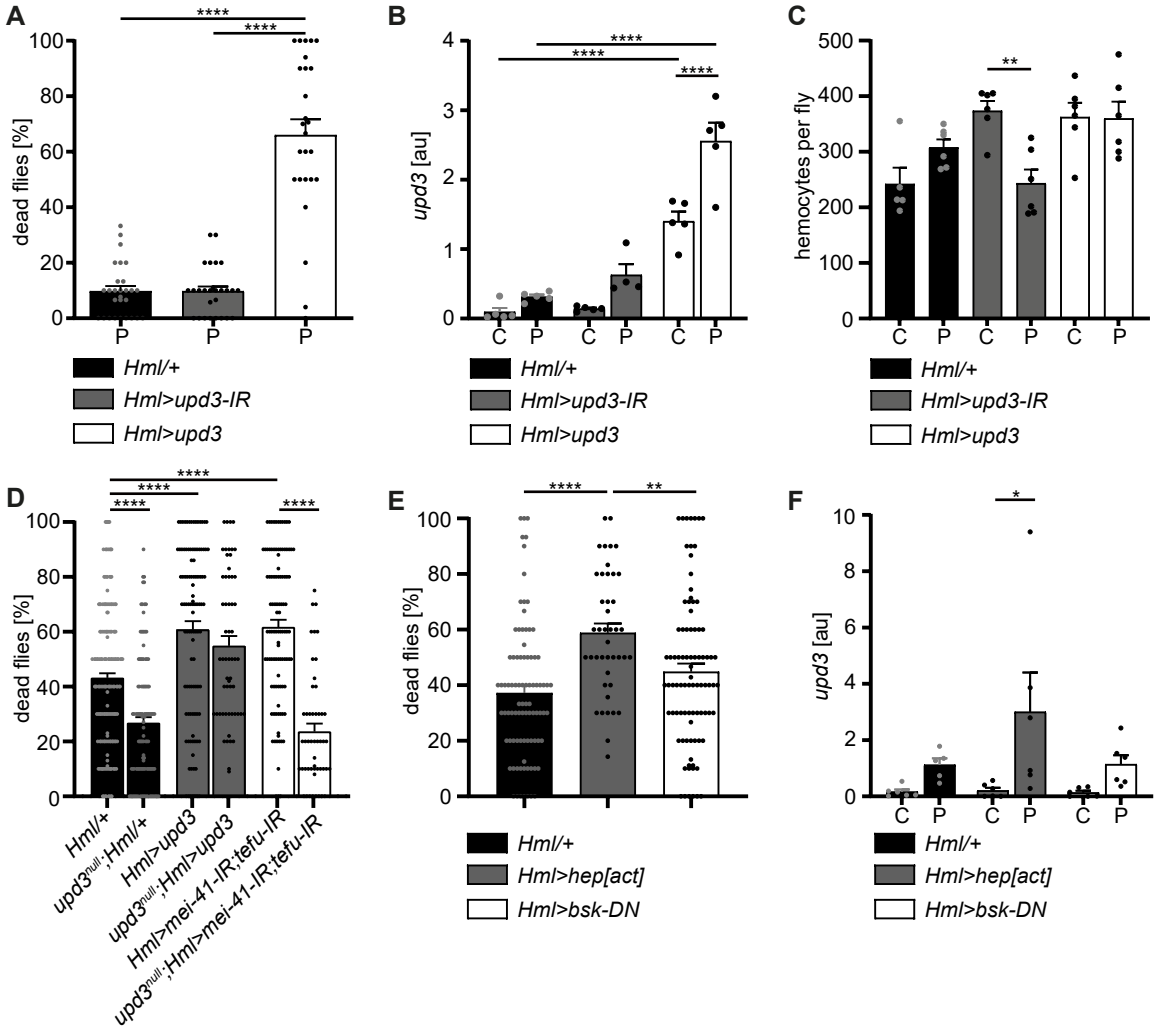
A
dead flies [%]
P
Hml/+
Hml>upd3-IR
Hml>upd3
B
upd3 [au]
C
P
C
hemocytes per fly
D
dead flies [%]
Hml/+
upd3^null;Hml/+
Hml>upd3
upd3^null;Hml>upd3
Hml>mei-41-IR;tefu-IR
upd3^null;Hml>mei-41-IR;tefu-IR
E
dead flies [%]
Hml/+
Hml>hep[act]
Hml>bsk-DN
F
upd3 [au]
C
P
Hml/+
Hml>hep[act]
Hml>bsk-DN

Figure 6